Coupling of Electrophysiology and Mechanics of Heart Muscle

Thesis

Submitted in partial fulfillment of the requirements of BITS F421T

BY

Ankush G K

2017B5A41552H

Under the supervision of

Dr. Yong Wang

Group Leader

Max Planck Institute for Dynamics and Self-Organization

&

co-supervision of

Dr. Nitin Ramesh Kotkunde

Assistant Professor

BITS Pilani Hyderabad Campus

BITS Pilani
Hyderabad Campus

BIRLA INSTITUTE OF TECHNOLOGY AND SCIENCE, PILANI

HYDERABAD CAMPUS

(December, 2021)

ACKNOWLEDGEMENTS

First and foremost, I have to thank my thesis supervisor Dr. Yong Wang, who has patiently and kindly been supportive in every step of the way. It was a privilege to work under his guidance and an amazing opportunity to work on such interestnig and impactful topic. Working remotely from home during a worldwide pandemic was a challenge, and I could not have asked for a better guide in these extraordinary circumstances.

I would also like to thank Mr. Yunxiao Zhang, who is a PhD candidate working with Dr. Y. Wang. Mr. Zhang has helped me along the way with necessary technical information and several resources to learn from whenever I was in need, without which it would not have been possible for me to move forward. I am also thankful to the other group members of the Biofluidics and Biomechanics group at Max-Planck Institute for Dynamics and Self-organization (MPIDS) for some engaging presentations and discussions on fascinating topics.

I am grateful to my co-supervisor, Dr. Nitin Ramesh Kotkunde for easing up the academic process at BITS Pilani Hyderabad Campus where I was given the opportunity to pursue my thesis at MPIDS.

Finally, I would like to express my gratitude to my family who has been supportive of me throughout and especially during the pandemic which has affected everyone in some way. The peace of mind and safety, without which engaging in research activity would have been strenuous, was a privilege offered by my family.

Thank you.

Abstract

Heart beats several thousand times a day and keeps on doing it without wearing out. This says something about the property of the material heart is made of. To understand how the heart functions, we need to look at its cells, its structure, the processes that take place in it, the underlying properties. Heart contracts and pumps blood throughout the body. This contraction is a consequence of the propagation of an electrical signal originating at one part of the heart. This signal affects how the heart deforms and the deformation in turn affects how the signal is propagated. Modeling these phenomena requires experimental data and mathematical models that fit. Mechanical testing of the heart muscle shows a non-linear elasticity and the presence of fibres inside makes it challenging to build theoretical models that mimic the reality. At first, this thesis covers the action potential propagation and solid mechanics of the heart muscle separately. This is done by covering the two-dimensional simulations of the action potential wave propagation for plane, radial and square-corner stimulus, and three dimensional simulation of both passive and active deformation of the domain. The basics of Solid Mechanics is also covered where all the necessary conceptrs and quantities are defined and all the necessary models are dicussed. Nearly incompressible, transversely isotropic, hyperelastic material model is explored in this thesis for the deformation and a modified monodomain Fitz-Hugh Nagumo model is used for the electrophysiology part. Then, the thesis explores the One-Way coupling where the excitation induces deformation of the domain. Two-dimensional simulations of the coupling with plane and radial stimulus with different fiber orientations is covered. Three-dimensional simulations of the coupling with plane and radial stimulus with different combinations of fiber orientation is also discussed. The results in this thesis is compared to existing results from a paper and comparisons are drawn out. Further possible improvements to the model is proposed.

Table of contents

1 An Overview

1.1 Why model Heart?

Before getting into the actual topic of this thesis, it would be a bit easier to start with why do this work at all. Answering the question, in my opinion, there are two main reasons to model the Heart, not only human hearts, but hearts in general. First reason is that heart is probably the most important organ in a living organism. It becomes a natural curiosity to learn more about the thing which is keeping us alive. This curiosity has led us to what we learn about human hearts in our biology courses. We know that human heart is a fist-sized, 230-340g heavy "machine" that collects and pumps blood to different parts of the body via blood vessels. It is located inside the thorax, between the lungs, and inside pericardial sac. It is four-chambered, where the right side pumps deoxygenated blood through lungs back to heart, while the left side pumps oxygenated blood all around the body. The four chambers are two atria and two ventricles which are separated by atrial and ventricular septum respectively.
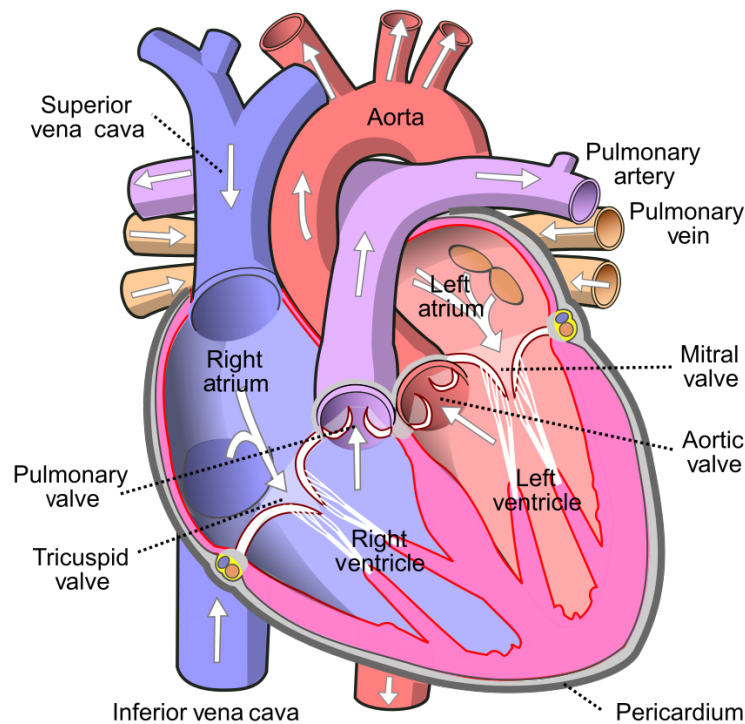
Figure 1. Diagram of a human heart with its valves, veins and arteries. The white arrows indicate the normal direction of blood flow. Image taken from Wikimedia Commons, the free media repository.

The second reason for modeling heart is that heart diseases are one of the leading causes of death in the world [19][13]. Many treatments require surgeries. Many go untreated because of lack of resources. To increase the success of surgeries and find new ways to treat Cardiovascular diseases

(CVD), we need to know how the heart functions. The next best place to test our understanding of the heart is to replicate it with the help of mathematical models and simulate their functions. There has been tremendous progress in this field with detailed experimental data and high-performance computers, leading to personalized health-care [10][1]. Conveniently, both these reasons need us to look into some aspects of the working of heart that will be covered in this thesis.

1.2   What is the Heart made of?

The heart wall is comprised of three layers: *endocardium*(inner), *myocardium*(middle), and *epicardium*(outer). These layers are enclosed in a double-membraned bag called *pericardium* (see Figure (2).) The focus of this thesis will be on the *myocardium*. Myocardium, also known as *cardiac muscle*, is a striated muscle tissue which is completely surrounded by a layer of *collagen*. This muscle structure is complex which wraps and swirls around the roots of blood vessels for efficient blood pumping.
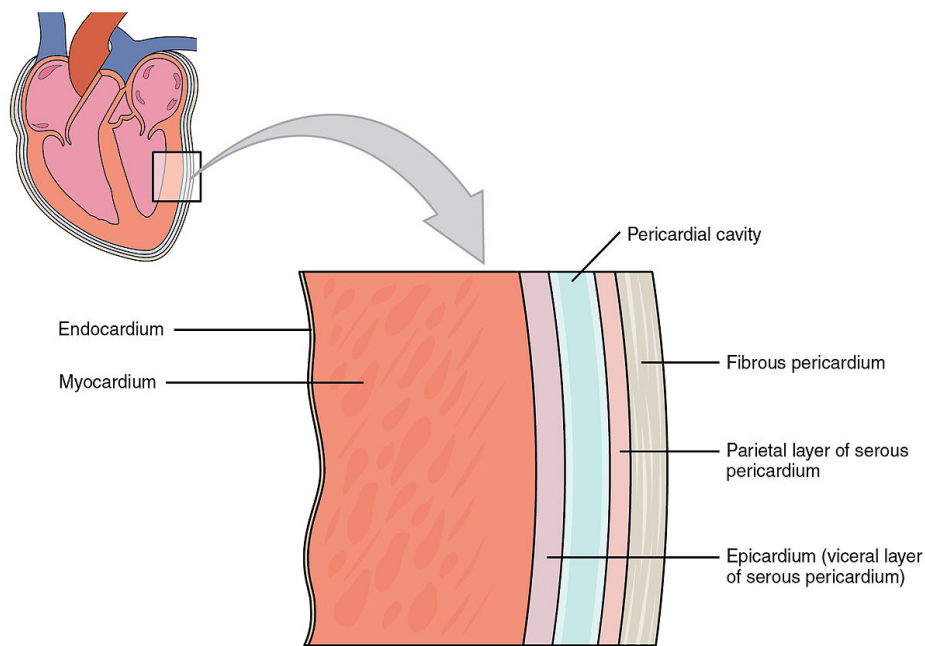

Figure 2. Heart layers. Image taken from: Anatomy & Physiology, Connexions Web site. http://cnx.org/content/col11496/1.6/

There are two different types of cells in the myocardium: (i) muscle cells (*myocytes)* which help in contraction, and (ii) pacemaker cells which help in conduction of electrical signals. Pacemaker cells are a type of muscle cell which have lost the ability to contract. They have the ability to generate electrical impulses by exchange of ions without any external factor, and this is known as *Autorhythmicity*. These electrical impulses travel to the myocytes in other regions of the heart which leads to their contraction. Going deeper into the structure of the myocytes, we see that they are roughly rectangular where each cell is joined to the other by *intercalated disks*. These cells are

surrounded by *extracellular matrix*. Each of these cells contain *myofibrils* which house the proteins *actin* and *myosin*. These proteins together form *sarcomere* which is the fundamental contractile unit of the system (See Figure (3).). Details of the dynamics of the contractile system will be covered in subsection 1.3.2. Apart from these cells, there are several other kinds of structures which make up the heart's valves, vessels, fibres, etc. which will not be a part of this thesis. Fibers are major structures in the heart muscles whose orientation plays a role in the stiffness and this will be covered in the later section.
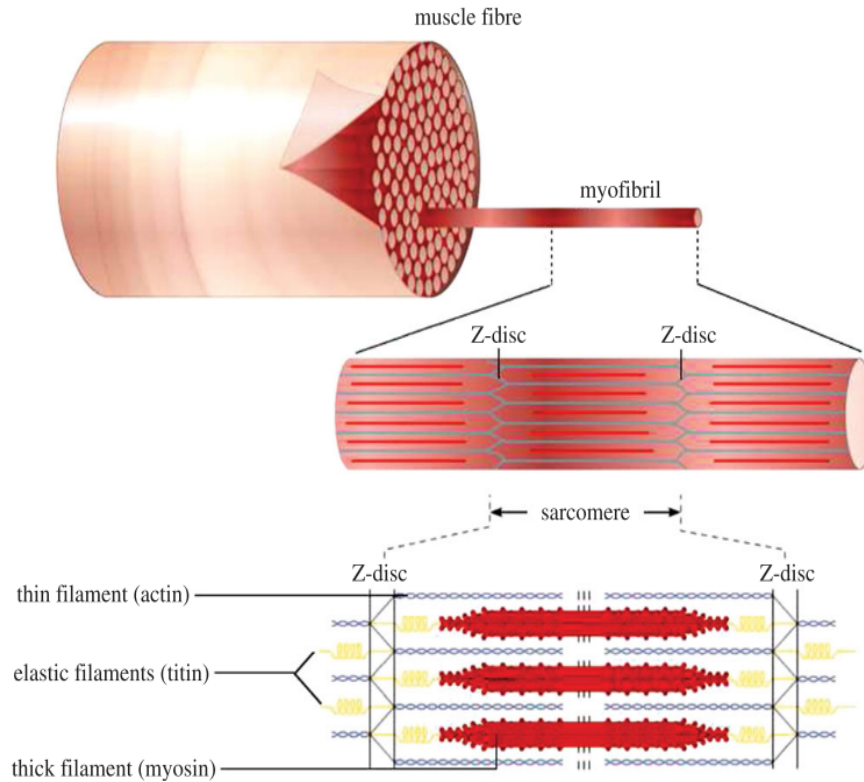
Figure 3. Myocyte structure. Image taken from [18]

1.3 What makes the Heart different?

The most unique thing about the heart, which is also the reason how it works the way it does, is the coupling between the contraction of myocytes and the propagating electrical impulse originated in pacemaker cells. To understand how they are coupled, first we need to understand each of these processes individually.

1.3.1 Action potential generation and propagation

The primary pacemaker cells are situated in *Sino-Atrial Node* (SAN). The SAN generates periodic electrical impulses on its own. This thesis will not cover the mechanism behind this autorhythmicity. The impulse is propagated throughout the heart via the conduction system as seen in Figure (4). This leads to the electrical impulse reaching the myocytes. The myocytes, at their resting state, have high concentration of K^+ ions and low concentration of Na^+ , Ca^{++} ions inside the cell(intracellular, i). Outside the cell(extracellular, e), the concentration of Na^+, Ca^{++} is high and that of K^+ is low. This means that, at rest, inside of the cell is more negative than the outside and the value of the potential across the cell membrane : *Trans-membrane Potential* (V_m)=$V_i - V_e$ is $-85\,\mathrm{mV}$. When the impulse from the pacemaker cells reaches the myocyte, it raises V_m slightly to a less negative value until a *Threshold Potential* is reached. On reaching this *Threshold Potential*, the Na^+ ion channel opens up and all the Na^+ ions follow the concentration gradient to move from extracellular to intracellular region at a high rate of flow. This causes a spike in the V_m value. While this happens, Ca^{++} ion channel also opens up and the Ca^{++} move in, but slowly. This is the *Depolarization* phase. The V_m cannot increase indefinitely. It reaches a *Maximum Potential* value when the Na^+ channel closes and the Na^+ influx stops. At this point, the K^+ channel opens up and K^+ ions start to move out. However, Ca^{++} ions are still moving in. The outflux causes the V_m to dip a little. This is the *Early Repolarization* phase. Soon, the influx of Ca^{++} will balance the out-flux of K^+ ions and the V_m value reaches a *Plateau*. During this stage, the Ca^{++} moving into the cell triggers the release of further more Ca^{++} ions from the *Sarcoplasmic Reticulum*. This is known as the *Calcium Induced Calcium Release.* This is when the contraction of the muscle takes place. This contraction is induced by the electrical impulse, so it is the *excitation induced contraction* and the mechanism behind this will be covered in the next subsection. Now a point is reached where the Ca^{++} channel closes but the K^+ ions keep moving out. This leads to V_m reaching its resting value. This is the *Repolarization* phase.
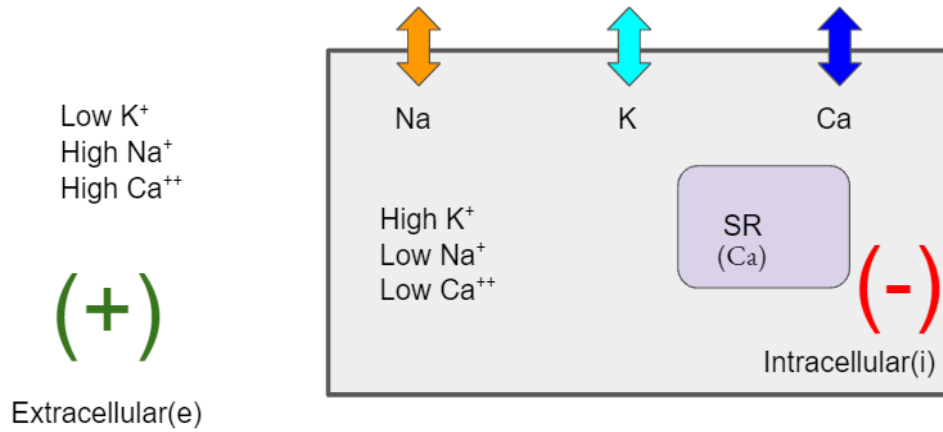

Figure 4. A crude representation of a cardiomyocyte (rectangular region) at its resting state, with Na, K, and Ca ion channels. The double-sided arrows represent the voltage-gated ion channels for the corresponding ions. SR: Sarcoplasmic Reticulum.

When the resting state is reached, some ions flow into the neighboring myocytes and this cycle begins again leading to the propagation of the electrical impulse. All of these phases can be plotted as a potential vs time graph and we call it **Cardiac Action Potential** as seen in Figure (5). More

details on the mechanism of action potential generation in pacemaker cells and in various other parts of the heart can be found in [20].
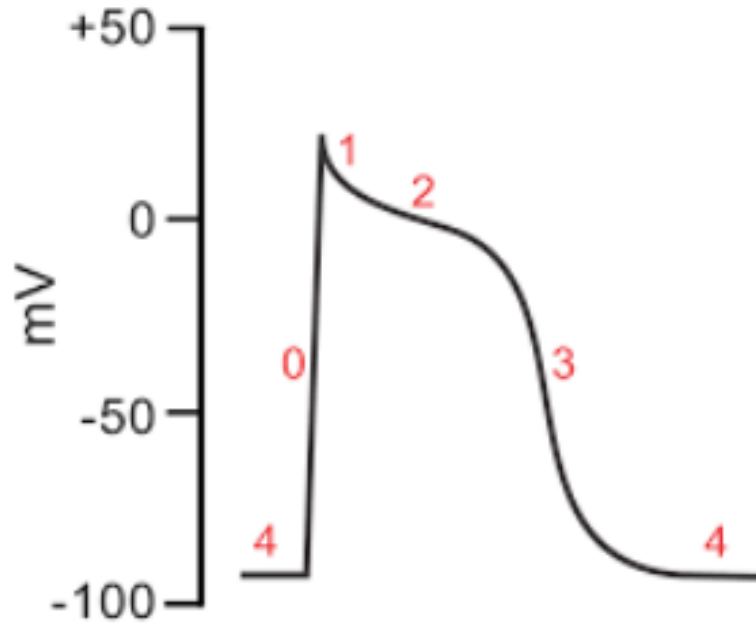

Figure 5. The Cardiac Action Potential. 0: Depolarization phase, 1: Early Repolarization phase, 2: Plateau phase, 3: Repolarization phase, 4: Resting potential. Taken from https://www.cvphysiology.com/Arrhythmias/A006

1.3.2 Excitation induced contraction

We saw in the previous subsection that the contraction of the myocytes happens during the *plateau* phase when there is Calcium triggered Calcium release from the Sarcoplasmic Reticulum (SR). SR surrounds the myofibrils (see Figure (6)). Each myofibril is made up of, *A band* where the thick myosin protein and thin actin protein overlap, and *I band* with only actin. The A band is at the centre of the sarcomere. Each sarcomere is bounded by *Z disks* where the actin is held. Myosin is present between two actin filaments. During the Calcium triggered Calcium release, the calcium ions bind to a protein Troponin which forces the Tropomyosin to move and expose the binding site. The myosin heads then bind to actin leading to a sliding dynamic. This sliding pulls the *Z disks* closer which results in contraction of myocyte. When the action potential propagates throughout the heart, it leads to contraction of the myocytes in its wake, which is how the heart gets the force to pump blood. This type of deformation which is induced by the excitation of the

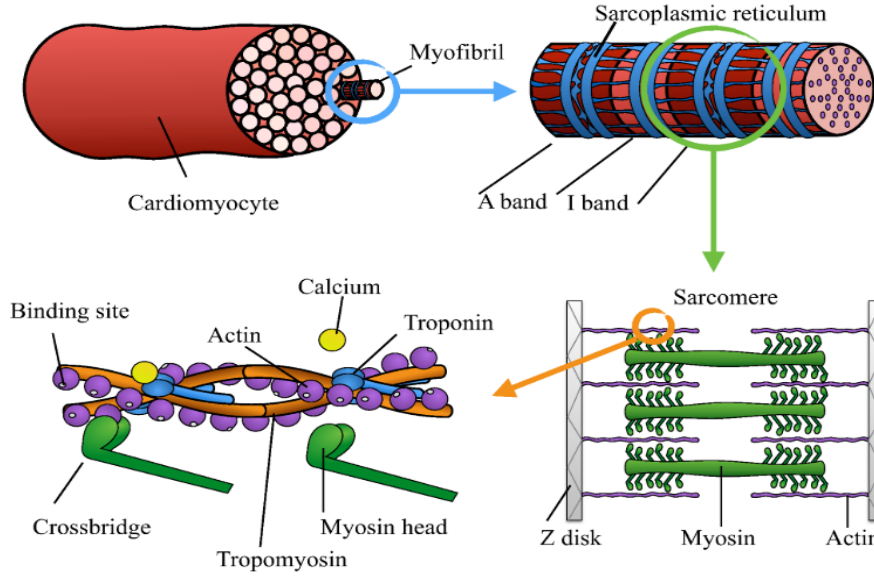myocytes is also known as **_Active Deformation_**.

Figure 6. Representation of cardiomyocyte contractile system. Image taken from [15].

From the above two subsections, it can be seen that electrical impulse and contraction of myocyte are interrelated and inter-dependent. Any change in the action potential propagation will affect the way in which the heart deforms and the deformation of the heart stretches/compresses the myocyte which in turn affects the propagation of the action potential. This is called _two-way coupling_.

1.3.3 Non-linear elasticity and orthotropy

This thesis will focus only on the myocardium, especially the ventricular myocardium. Usually, to determine the properties of a material and understand the structure inside it, we perform few mechanical tests like axial tests or shear tests. When such tests are performed on normal elastic materials, we get a linear relationship between stress and strain. But when such tests are performed on soft tissue like material [6][14], they show different behavior. Stress-strain relationship are non-linear. Later, it was found out that this behavior was due to the presence of fibers. Unique characteristic about fibers is that they tend to have a preferred direction. Figure (7) shows the stress strain response of skin which has collagen fibers present. This plot is representative of many kinds of soft tissue materials. The morphology of the fiber at different stages of testing influences how the tissue responds. This is also true for the heart tissue. At different levels of thickness of the heart muscle tissue, the orientation of the fibers vary. Biaxial extension tests (see Figure (9)) were performed which suggested that myocardial tissue is transversely isotropic. But later, shear tests(see Figure 10) in different orientations showed the material in the myocardium to be _orthotropic_. This means that typical tests done on normal materials are not enough to characterize the properties of myocardium. Although the presence of water in the heart tissue can make it viscoelastic, it is difficult to consider it so for modeling purposes. Close enough to reality is to consider them _hyperelastic_ materials.
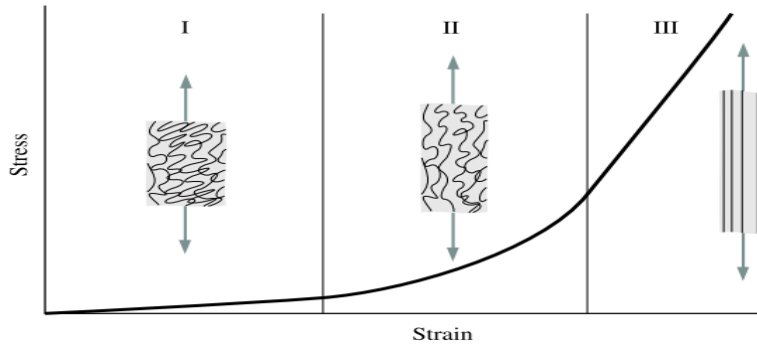
Figure 7. Stress strain curve for skin with collagen fiber arrangements. Taken from https://biome-chanics.stanford.edu/me338/me338_project02.pdf
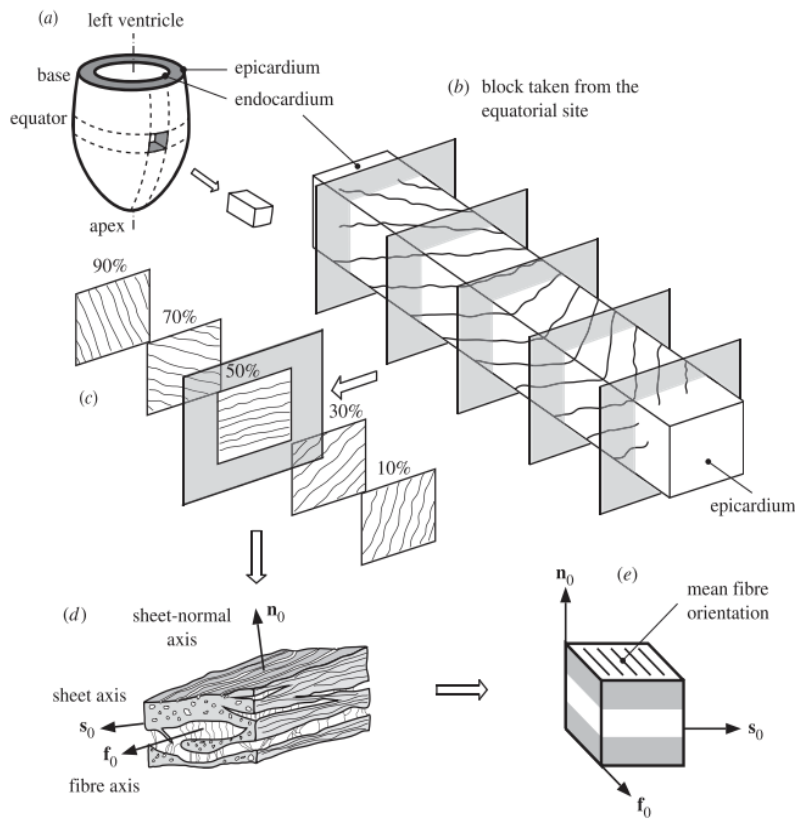

Figure 8. Schematic diagram of: (a) the left ventricle and a cutout from the equator; (b) the structure through the thickness from the epicardium to the endocardium; (c) five longitudinal– circumferential sections at regular intervals from 10 to 90 per cent of the wall thickness from the epicardium showing the transmural variation of layer orientation; (d) the layered organization of myocytes and the collagen fibres between the sheets referred to a right-handed orthonormal coordinate system with fibre axis f, sheet axis s and sheet-normal axis n; and (e) a cube of layered tissue with local material coordinates (X1,X2,X3) serving as the basis for the geometrical and constitutive model. Image and caption taken from [9].

Ventricular myocardium has complicated structure where myocytes are organized in layers separated by planes. This is *laminar structure* which is characterized by axes aligned (i) with myocyte direction(f), (ii) transverse to myocyte axis(s) and (iii) normal to the layer(n). Shear tests in each of these directions produce different response as seen in Figure 10. This difference in

responses in three different directions is the proof that myocardium is *orthotropic*.

(a)

(b)

(c)
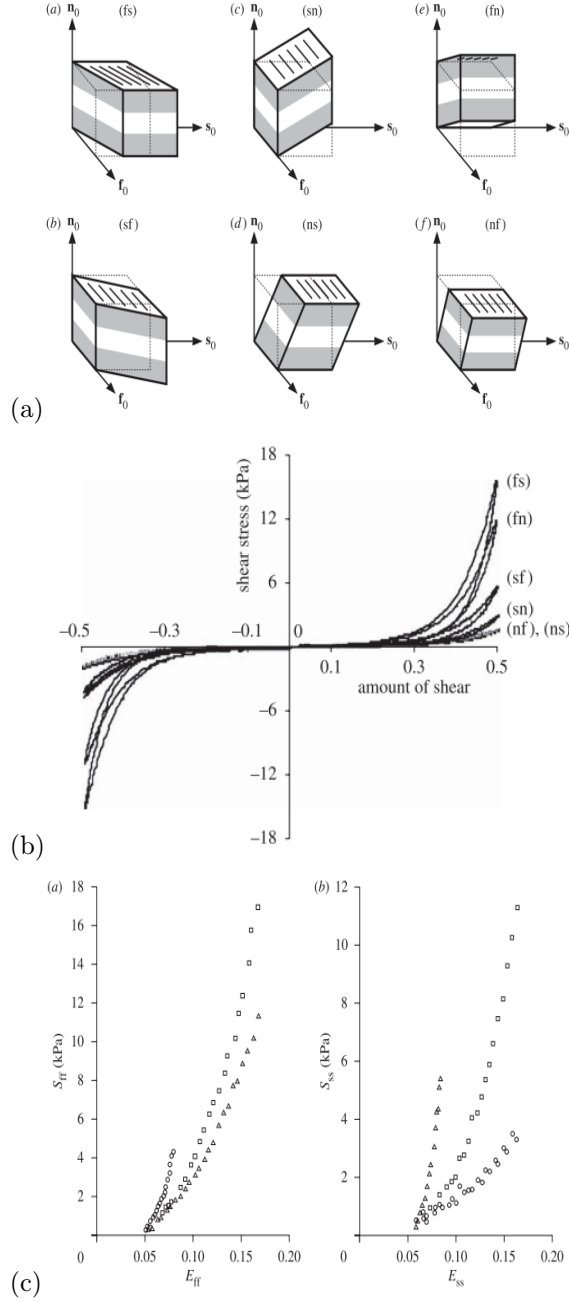
Figure 9. (a) Shear tests in different directions. (b) Shear responses in different directions in triaxial shear test. (c) Stress-strain curves for different strain ratios from the biaxial testing. Images taken from [9][21]

These properties of the myocardium which respond to external load or shear belong to the **Passive Deformation**. For modeling the heart muscle, we need to take into account, the action potential propagation, active deformation and passive deformation. There is also fluid mechanics side of the problem which deals with the blood flow and its effect on the above properties which will not be covered in this thesis. Let's take a look at how we can model these using mathematical equations.

2 Mathematical Modeling of Electrophysiology of the Heart Muscle

We have seen the theory behind the action potential generation and propagation through myocytes. This section deals with mathematical modeling of the same.

2.1 Model of an excitable tissue

The membrane of the myocyte can be imagined as an electrical circuit where the cell membrane acts like a capacitor. The voltage-gated ion channels with potential difference due to the concentration gradient (*Nernst Potential*) act like batteries in parallel to the capacitor (see Figure (10)). The flow of ions give rise to their own current which is called *ionic current*(i_{ion}). This circuit is connected with several similar ones which represent the connected myocytes. The stimulus is given in the form of current(i_{stim}) in the extracellular region.
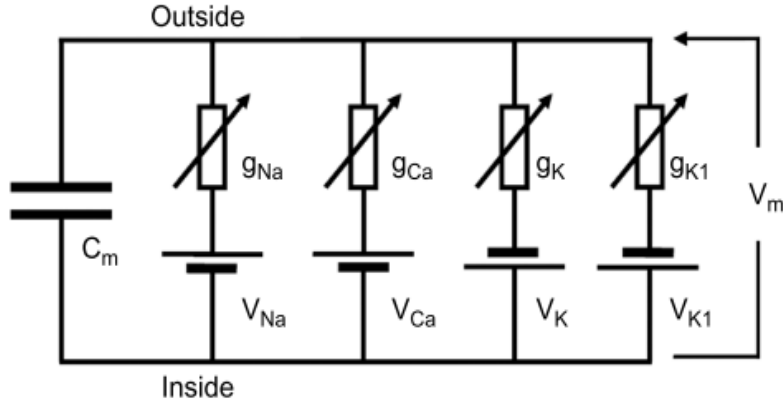
Figure 10. Equivalent electrical circuit for a cardiac cell membrane. g: Nernst potential for the corresponding ion. Image taken from [2].

Total current flow in the circuit/membrane can be expressed as

$$i_m = i_{\text{capacitive}} + i_{\text{ionic}} \tag{1}$$

$$i_m = C_m \frac{\partial V_m}{\partial t} + i_{\text{ionic}} \tag{2}$$

where C_m is the membrane capacitance, $V_m = V_i - V_e$ is the trans-membrane voltage, i_{ionic} is the combination of Na, K and Ca currents. Using Maxwell's equations and conservation of current principle, we can write

$$\nabla \cdot (-\sigma \nabla V) = i \tag{3}$$

where σ is the conductivity.

2.1.1 Bi-domain Model

Applying Eq. (3) to the excitable tissue model gives us

$$\nabla.(-\sigma_e \nabla V_e) = \beta(i_m) \qquad \text{(extracellular \ domain)} \tag{4}$$

$$\nabla.(-\sigma_i \nabla V_i) = -\beta(i_m) \qquad \text{(intracellular \ domain)} \tag{5}$$

Substituting Eq. (2) for i_m

$$\nabla.(-\sigma_e \nabla V_e) = \beta\left(C_m \frac{\partial V_m}{\partial t} + i_{\text{ionic}} \right) \qquad \text{(extracellular \ domain)} \tag{6}$$

$$\nabla.(-\sigma_i \nabla V_i) = -\beta\left(C_m \frac{\partial V_m}{\partial t} + i_{\text{ionic}} \right) \qquad \text{(intracellular \ domain)} \tag{7}$$

where β is the surface-to-volume ratio. These are the *reaction-diffusion equations.* Although this model represents a detailed model of cardiac tissue, it is a system of coupled differential equations which is difficult to integrate numerically making it computationally expensive. For this reason, we can simplify this system to make it easier to use.

2.1.2 Mono-domain Model

In this model, the extracellular domain is assumed to be grounded. In other words $V_e = 0$. Applying this change to previous model, we get

$$\nabla.(-\sigma \nabla V_m) = -\beta\left(C_m \frac{\partial V_m}{\partial t} + i_{\text{ionic}} \right) \tag{8}$$

This is much easier to solve numerically and faster too.

2.2 Ionic current model

There are several models to simulate the dynamics of the Na, K and Ca currents in the cell. The main aim of an ionic current model is to give us the action potential dynamics as close to Figure (6) as possible. One of the earliest models was built by Hodgkin and Huxley in [8]. All other models are either based on this or use this as a reference to build a new one. But, there are simpler models which can be used for most of the purposes. In this thesis, Fitz-Hugh Nagumo (FHN) model is used [5][11].

2.2.1 Simplest Fitz-Hugh Nagumo Model

One of the simplest forms of FHN equation without the diffusion term is used here to model the action potential. An external stimulus is added to the ionic current term in the model.

$$\frac{\partial V_m}{\partial t} = i_{\text{ionic}} + i_{\text{stim}} - w \tag{9}$$

$$\frac{\partial V_m}{\partial t} = V_m(V_m - V_{\text{th}})(V_{\text{max}} - V_m) + i_{\text{stim}} - w \tag{10}$$

$$\frac{\partial w}{\partial t} = \epsilon(V_m - \gamma w) \tag{11}$$

where V_{th} is the threshold potential above which V_m spikes and below which V_m dies down, V_{max} is the maximum potential limiting the rise of V_m, w is the blocking mechanism which brings V_m to its resting value, ϵ and γ are the blocking parameters that control the value of w. These equations are mathematical representations of the theory discussed in subsection 1.3.1. This was solved in MATLAB with the dimensionless values for the parameters as follows: V_{th}=0.25, V_{max}=1, initial value of V_m=0.3, initial value of w=0, ϵ=0.005, γ=2 and i_{stim}=0.075, which gave a plot as in Figure
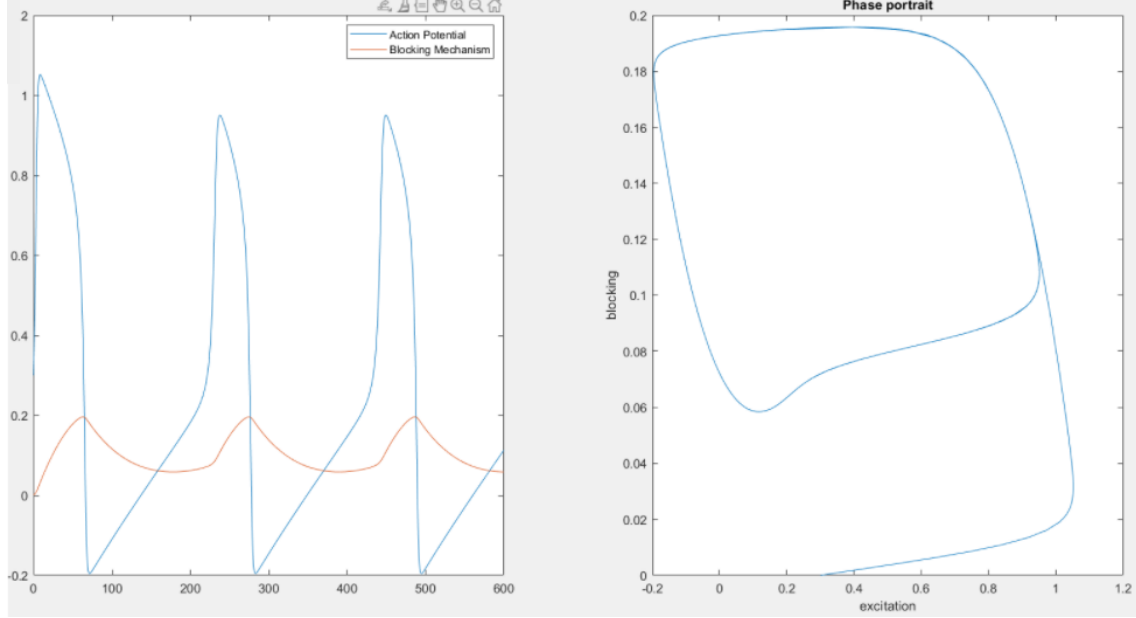

Figure 11. (Left)Action potential propagation with time showing the rise and fall of action potential with blocking mechanism and (Right) the phase portrait of blocking mechanism vs action potential.

As we can see, the action potential in Figure (11) does not have the same shape as that in Figure (5). This is because this FHN model is a much simpler one. There are several forms of FHN models which have a few extra terms to make the action potential look as realistic as possible. We will look at one of those forms of FHN model.

2.2.2 Modified Fitz-Hugh Nagumo Model

We will be dealing with the modified Fitz-Hugh Nagumo model formulated by Rogers-McCulloch [16] for the cardiac action potential. We will be looking at the mono-domain model because of its computational ease to use. The equations are as follows

$$\nabla.(-\sigma\nabla V_m) = -\beta\left(C_m\frac{\partial V_m}{\partial t} + i_{\text{ionic}}\right) + i_{\text{stim}} \tag{12}$$

$$\frac{\partial u}{\partial t} = e(V_m - du - b) \tag{13}$$

with

$$i_{\text{ionic}} = c_1(V_m - a)(V_m - A)(V_m - B) + c_2 u(V_m - B)$$

$$\sigma = \begin{pmatrix} \sigma_x & 0 & 0 \\ 0 & \sigma_y & 0 \\ 0 & 0 & \sigma_z \end{pmatrix} \qquad \text{for } 3D \text{ domain}$$

where u is the blocking mechanism, σ is the conductivity tensor with the components being the principal conductivities along x-,y- and z-axis. i_{stim} is the external stimulus applied per unit

volume. $A, B, a, b, d, e, c_1, c_2$ are parameters that describe the electrical activity whose values can be found in Figure (12).

Parameter	Value	Parameter	Value
A	$55\,\mathrm{mV}$	c_2	$400\,\mu\mathrm{S cm}^{-2}$
B	$-85\,\mathrm{mV}$	C_m	$1\,\mu\mathrm{F cm}^{-2}$
a	$-66.8\,\mathrm{mV}$	β	$100\,\mathrm{m}^{-1}$
b	$-85\,\mathrm{mV}$	σ_{ex}	$0.1\,\mathrm{mS\,cm}^{-1}$
d	$140\,\mathrm{mV}$	σ_{ey}	$0.025\,\mathrm{mS\,cm}^{-1}$
e	$285.7\,\mathrm{V}^{-1}\,\mathrm{s}^{-1}$	σ_{ix}	$0.2\,\mathrm{mS\,cm}^{-1}$
c_1	$530\,\mathrm{S\,V}^{-2}\,\mathrm{m}^{-2}$	σ_{iy}	$0.1\,\mathrm{mS\,cm}^{-1}$

Figure 12. Modified FHN model parameters. Taken from [3].

Applying Eq. (12) and Eq. (13) to a two-dimensional 10cm x 10cm square domain and a three-dimensional 10mm x 10mm x 0.5mm domain, with the values of the parameters as in Figure (12). Figure 13 and Figure 15 show the meshing implemented in both 2D and 3D domains respectively. Physics-controlled mesh of Normal element size in COMSOL is used throughought this thesis. COMSOL's General Form PDE Physics is used to formulate FHN equations (Eq. (12) and Eq. (13)). Zero flux boundary condition is given to all the outer boundaries of the domain. The initial values for V_m and u is given as $-85\mathrm{mV}$ and 0 respectively. The stimulus i_{stim} of value $100\,\mathrm{Am}^{-3}$ is applied to (i) a 10cm x 1cm rectangular patch, (ii) a circular region of 0.5cm radius, and (iii) a 0.5cm x 0.5cm square patch. The value of i_{stim} is zero in all other regions. For 2D simulations, the conductivity tensor has only the x- and y-components whose values, when changed, affect the propagation speed and shape of the action potential wave across the domain. On the other hand, in 3D simulations there is an extra z-component which also plays a role. The values can be varied to move from an isotropic to an anisotropic problem. A Time Dependent Study is initiated for times ranging from $t = 0s$ to $t = 0.6s$ with the time-step of $t = 0.001s$. COMSOL modifies the solvers according to the problem at hand and here MUMPS solver is used. Figure 14 and Figure 16   show the propagating action potential for different stimulus in a 2D and 3D domain respectively. These models only focus on the influence of differerent conductivities on the propagation and cannot be compared to experimental observations as that would require several different and more accurate ionic models. The results show the isotropic behaviour which can be seen in the symmetric propagation of the wave. Anisotropic behviour would mean that (i) the plane stimulus would generate a wave with curvature (ii) the radial stimulus would generate an elliptical wave, and (iii) the square-corner stimulus would generate a stretched quadrant shaped wave.
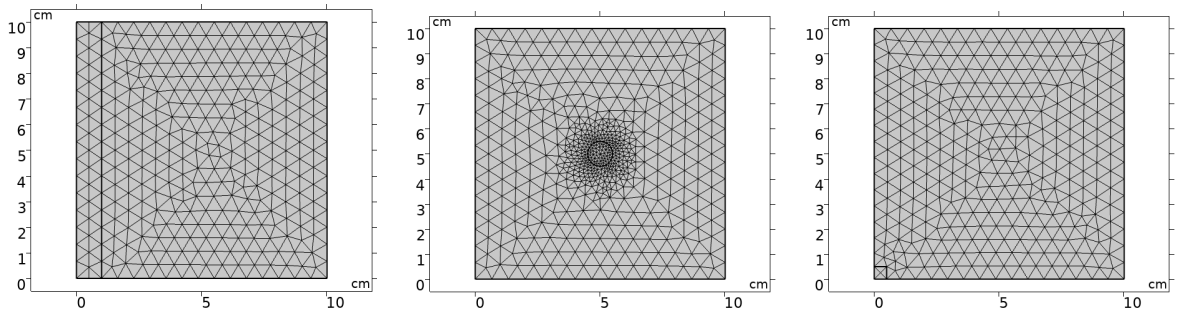

Figure 13. 2D Meshed domain for (left)plane, (middle)radial and (right)square-corner stimulus configurations
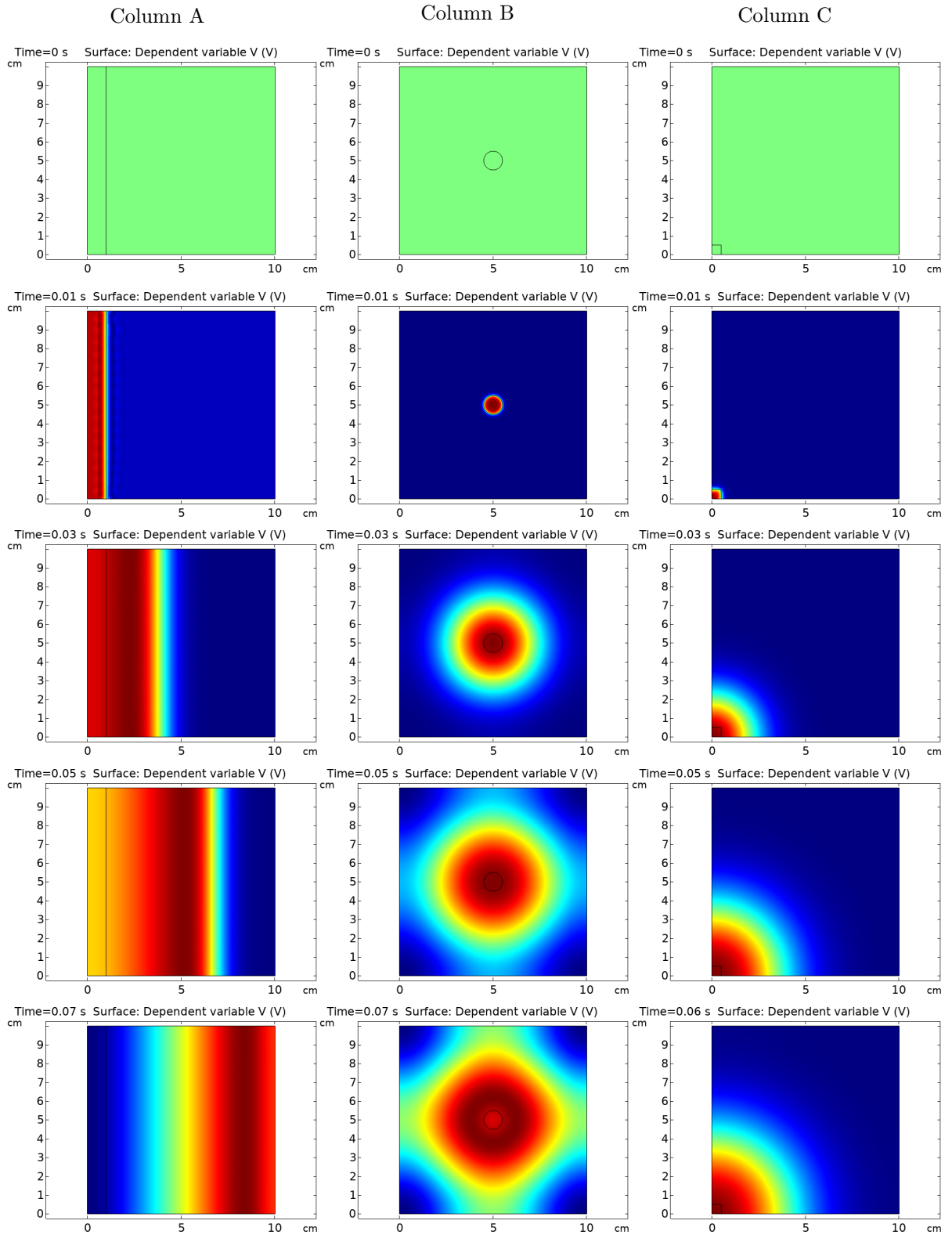
Figure 14. Propagating action potential in a 2D domain. Column A: Plane stimulus where the stimulus is given to the rectangular region near the left edge of the domain, **Column B:** Radial stimulus where the stimulus is given to the circular region at the center of the domain, and **Column C:** stimulus is given to the square-shaped region at the left-bottom corner of the domain.

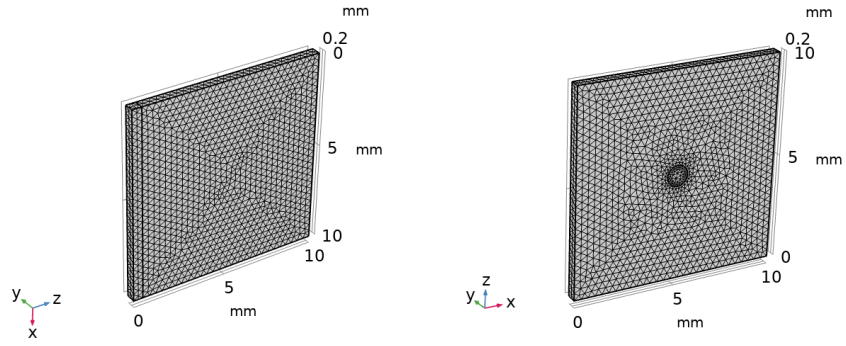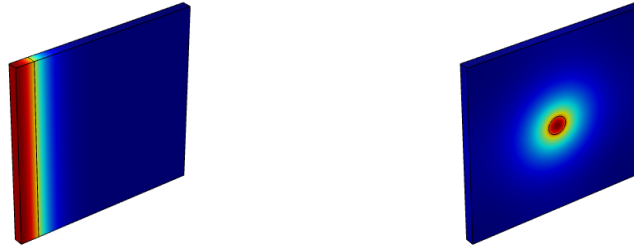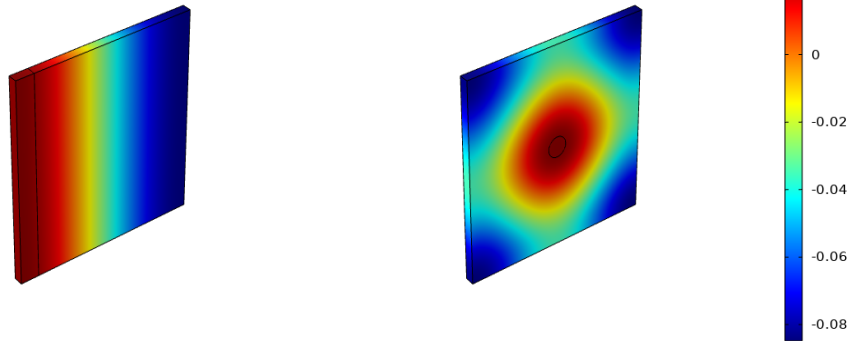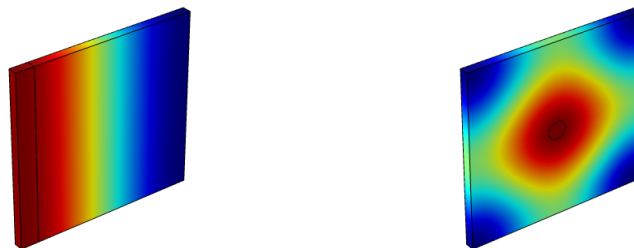**Figure 15.** 3D meshed domain for (left) plane and (right) radial stimulus configuration.

Figure 16. Propagating action potential in a 3D domain. Column A: Plane stimulus, **Column B** Radial stimulus. The colour bar indicates the Transmembrane Potential (V_m).

3 Mathematical Modeling of Mechanics of Heart Muscle

To understand how the heart muscle deforms and the properties discussed in Section 1.3.3, we need some foundational ideas on the mechanics of solids in general.

3.1 Basics of Solid Mechanics

3.1.1 Requirements to model a material

To model a material, we need four sets of relations

- Kinematic Relations   - that characterizes deformation

- Stress Equilibrium   - that tells us about the motion of the body

- Constitutive Relations - that relates two of the above

- Boundary Conditions

First, we will look at the Kinematic relations and stress equilibrium relations.

3.1.2 Stress and Strain
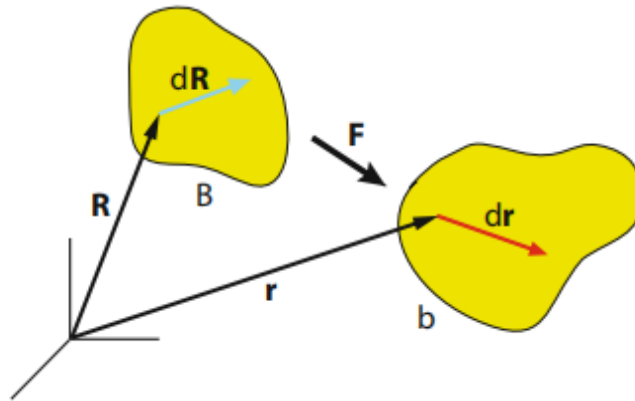
Figure 17. Deformation gradient tensor **F** is a transformation which relates the undeformed configuration with deformed configuration. Line element **dR** deforms to **dr**. Image taken from [17].

In solid mechanics, we always deal with two configurations of a body: *reference/initial/undeformed configuration* and *final/deformed configuration*. To capture how each and every point/line/volume on a body changes, we need to have a quantity that measures this change. Consider a vector **dX** in the reference configuration. When the body deforms, **dX** changed to **dx**. Uppercase letters used to describe the reference configuration and lowercase letters used

to describe the deformed configuration. This change is now written as $\mathbf{dx} = \mathbf{F.dX}$, where $\mathbf{F}$ is the *deformation gradient tensor*.

$$F = \frac{dx}{dX} = (\nabla x)^T \tag{14}$$

$$F = I + (\nabla u)^T \tag{15}$$

where $\boldsymbol{u}$ is the displacement vector $\Rightarrow \boldsymbol{x} = \boldsymbol{X} + \boldsymbol{u}$.

The deformation gradient tensor describes rigid body motion in addition to deformation. Consider a line element $\mathbf{dR}$ of length dL which deforms to a line element $\mathbf{dr}$ of length dl.

$$dL^2 = \mathbf{dR.dR} = \mathbf{dr.dr} = (\mathbf{dR}.\boldsymbol{F}^T).(\boldsymbol{F}.\mathbf{dR}) = \mathbf{dR}.\boldsymbol{C}.\mathbf{dR}$$

$$C = F^T.F \tag{16}$$

where $\mathbf{C}$ is the *right Cauchy-Green Deformation tensor* and it is symmetric. As the body deforms, the vectors get stretched and also a change in angle between them. Right Cauchy green deformation tensor describes that.

$$b = F.F^T \tag{17}$$

where $\mathbf{b}$ is the *left Cauchy-Green deformation tensor*.

$$E = \frac{1}{2}(C - I) = \frac{1}{2}(F^T.F - I) \tag{18}$$

where $\mathbf{E}$ is the *Lagrangian strain tensor*.

Consider an area element $\mathbf{dA}$ in the reference configuration which deforms to $\mathbf{da}$ in the deformed configuration. These two are related by Nanson's formula,

$$da = \mathbf{J}\mathbf{F}^{-T}dA \tag{19}$$

where $J = \det F$. Similarly, volume in reference configuration($\mathbf{dV}$) is related to that in deformed configuration ($\mathbf{dv}$) by

$$dv = JdV \tag{20}$$

When external loads are applied, we need to be able to quantify the forces acting. We use stresses which are force per unit area, to represent the applied loads.
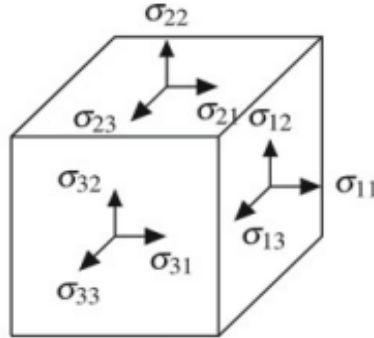

Figure 18. Stress state.

Consider an infinitesimal cube. Nine stress components σ_{ij} $(i, j = 1, 2, 3)$ acts on the faces of the cube. These can be written as

$$\boldsymbol{\sigma} = \begin{pmatrix} \sigma_{11} & \sigma_{12} & \sigma_{13} \\ \sigma_{21} & \sigma_{22} & \sigma_{23} \\ \sigma_{31} & \sigma_{32} & \sigma_{33} \end{pmatrix}$$

which is known as *Cauchy stress*.

The stress distribution within a solid can be formulated with Newton's second law of motion,

$$\rho \frac{\partial^2 \boldsymbol{u}}{\partial t^2} = \nabla . \boldsymbol{\sigma} + \boldsymbol{f} \tag{21}$$

where $\boldsymbol{f}$ is the body force per unit volume. This equation is *Cauchy momentum equation*. When dealing with deformations, the area of the reference configuration differs from that of the deformed configuration. In such cases, the more precise definition of *Cauchy stress* or *true stress* is force per unit deformed cross-sectional area. But it is not easy to calculate the deformed area everytime experimentally, so a useful measure is *1st Piola-Kirchhoff stress* ($\boldsymbol{P}$) or *engineering stress*, which is defined as force per unit undeformed cross-sectional area. It is to be noted that 1st P-K tensor is a fictitious tensor. Physically, Cauchy stress is the only meaningful quantity. We will also make use of another pseudo stress called *2nd Piola-Kirchhoff stress* ($\boldsymbol{S}$) which is a symmetric tensor and can be useful for easy computations.

$$\boldsymbol{\sigma} = J^{-1} \boldsymbol{F} . \boldsymbol{P} = J^{-1} \boldsymbol{F} . \boldsymbol{S} . \boldsymbol{F^T} \tag{22}$$

Any of the three stresses can be used depending on the problem. But the final stress representation has to be in terms of Cauchy stress.

In the study of materials, we always need to know the extreme stresses, both magnitude and directions, that the body can withstand. To calculate such extreme (maximum or minimum) cauchy stress on a body, we use the *Lagrange Multiplier method* where we solve an eigenvalue problem and obtain a characteristic polynomial of $\boldsymbol{\sigma}$

$$\lambda^3 - I_1 \lambda^2 + I_2 \lambda - I_3 = 0 \tag{23}$$

where λ represents the three eigenvalues which are the *principal normal stresses* and I_1, I_2, I_3 are the three principal invariants of $\boldsymbol{\sigma}$.

$$I_1(\boldsymbol{\sigma}) = \mathrm{tr}\, \boldsymbol{\sigma} = \lambda_1 + \lambda_2 + \lambda_3 \tag{24}$$

$$I_2(\boldsymbol{\sigma}) = \frac{1}{2}[\mathrm{tr}(\boldsymbol{\sigma})^2 - \mathrm{tr}(\boldsymbol{\sigma^2})] = \lambda_1 \lambda_2 + \lambda_1 \lambda_3 + \lambda_2 \lambda_3 \tag{25}$$

$$I_3(\boldsymbol{\sigma}) = \det \boldsymbol{\sigma} = \lambda_1 \lambda_2 \lambda_3 \tag{26}$$

These relations hold good for any type of material, so they cannot be used to distinguish between different materials. We need some form of a relationship between stress and strain which can tell us more about the material we are dealing with. These are the *constitutive relations*. In linear elasticity, this relation is written as

$$\boldsymbol{\sigma} = \boldsymbol{c} . \boldsymbol{\epsilon}$$

where $\boldsymbol{c}$ is a constant. But for general cases, $\boldsymbol{c}$ is a fourth-order tensor with 81 components.

3.1.3 Hyperelasticity

A *hyperelastic* material is the one for which there exists *Helmholtz free-energy function* W defined per unit reference volume. If the W is exclusively a function of $\boldsymbol{F}$, $W = W(\boldsymbol{F})$ then it is called *strain energy function*. Hyperelastic material are a subset of elastic material with stresses defined as

$$\boldsymbol{P} = \frac{\partial W(\boldsymbol{F})}{\partial(\boldsymbol{F})} \tag{27}$$

$$\Rightarrow \boldsymbol{\sigma} = J^{-1}\boldsymbol{P}\boldsymbol{F}^T = J^{-1}\frac{\partial W(\boldsymbol{F})}{\partial(\boldsymbol{F})}\boldsymbol{F}^T \tag{28}$$

To be able to use these equations in all situations, W needs to be *objective*, meaning that the function cannot vary for different frames of reference. If *objectivity* is taken into consideration, then by applying the polar decomposition on $\boldsymbol{F}$ as $\boldsymbol{F} = \boldsymbol{R}\boldsymbol{U}$, we can write

$$W(\boldsymbol{F}) = W(\boldsymbol{U}) \tag{29}$$

where $\boldsymbol{R}, \boldsymbol{U}$ are orthogonal rotation tensor and symmetric right stretch tensor respectively. Since, $\boldsymbol{C} = \boldsymbol{U^2}$ and $\boldsymbol{E} = \frac{1}{2}(\boldsymbol{U^2} - \boldsymbol{I})$, we can further write

$$W(\boldsymbol{F}) = W(\boldsymbol{U}) = W(\boldsymbol{E}) \tag{30}$$

Furthermore ,

$$\left(\frac{\partial W(\boldsymbol{F})}{\partial(\boldsymbol{F})}\right)^T = 2\frac{\partial W(\boldsymbol{C})}{\partial(\boldsymbol{C})}\boldsymbol{F^T} \tag{31}$$

So the piola-kirchhoff tensors can be written as

$$\boldsymbol{P} = 2\boldsymbol{F}\frac{\partial W(\boldsymbol{C})}{\partial(\boldsymbol{C})} \tag{32}$$

$$\boldsymbol{S} = 2\frac{\partial W(\boldsymbol{C})}{\partial(\boldsymbol{C})} = \frac{\partial W(\boldsymbol{E})}{\partial(\boldsymbol{E})} \tag{33}$$

3.1.4 Symmetry

There are certain properties which can impose constraint on the strain energy function which can help in revealing the property of the material. ***Isotropic*** materials are the ones where the properties relations remains the same in all directions. If we impose isotropy condition to hyperelastic materials, then we get a form of W which is invariant. ***Anisotropic*** materials have properties that are not the same in all directions. In ***Transversely Isotropic*** materials, the properties are symmetric about one axis which is normal to the isotropic plane. In this isotropic plane, the properties are same in all directions. ***Orthotropic*** materials have different properties along three mutually perpendicular directions with each axis having twofold rotational symmetry.
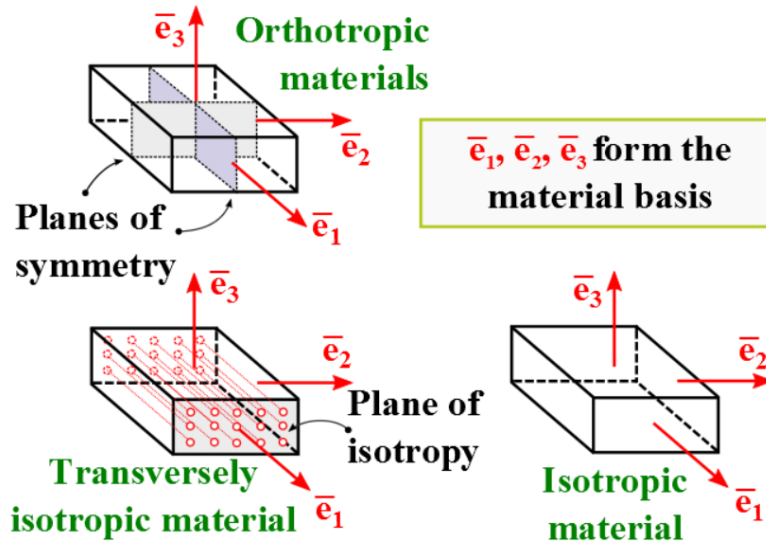
Figure 19. Symmetry in materials. Image taken from this site.

3.1.5 Compressibility

This is another form of a constraint imposed on the material. ***Incompressible*** materials are the ones which have no effect on their volume upon any kind of deformation. This condition is imposed by specifying $J = 1$. ***Compressible*** materials have an effect on their volume upon deformation. Due to the difference in behavior of the materials, it is convenient to separate the deformation into a *volumetric* part and an *isochoric* part. That means, $\boldsymbol{F}$ is multiplicatively split into *dilatational(volume-changing)* and *distortional(volume-preserving)* parts as

$$\boldsymbol{F} = J^{\frac{1}{3}}\bar{\boldsymbol{F}} \qquad \boldsymbol{C} = J^{\frac{2}{3}}\bar{\boldsymbol{C}} \tag{34}$$

where the $J^{\frac{1}{3}}, J^{\frac{2}{3}}$ are the volume-changing part and $\bar{\boldsymbol{F}}, \bar{\boldsymbol{C}}$ called the *modified deformation gradient* and *modified right Cauchy-green tensor* are the volume-preserving parts. A ***Nearly-Incompressible*** material is the one for which volume-preserving changes need less work than the volume-changing ones. Because of this decomposition, the strain energy function also changes to

$$W = W_{\text{iso}} + W_{\text{vol}}(J) \tag{35}$$

Similarly the 2nd piola-kirchhoff stress also becomes

$$\boldsymbol{S} = 2\frac{\partial W(\boldsymbol{C})}{\partial(\boldsymbol{C})} = \boldsymbol{S}_{\text{vol}} + \boldsymbol{S}_{\text{iso}} \tag{36}$$

3.2 Passive & Active Myocardium

We know that, for an *incompressible* material,

$$J = \det \boldsymbol{F} = 1$$

For a *nearly incompressible* material, it must be some function of J. We choose to use this,

$$W_{\text{vol}} = \kappa \left(\frac{(J-1)^2}{2} - \log J \right) \tag{37}$$

To reflect *orthotropy*, first we need to know how do we represent a material which has a preferred direction. From Eq. (16), we can write its principal invariants as

$$I_1 = \text{tr}\, \boldsymbol{C} \qquad I_2 = \frac{1}{2}[I_1^2 - \text{tr}(\boldsymbol{C}^2)] \qquad I_3 = \det \boldsymbol{C} \tag{38}$$

These are *isotropic invariants.* Now if the material has a preferred direction and let's denote it by $\boldsymbol{n_1}$, this means there is anisotropy in the material. More specifically, *transverse isotropy.* This introduces *transverse isotropic invariants* I_4, I_5

$$I_4 = \boldsymbol{n_1}.(\boldsymbol{C n_1}) \qquad I_5 = \boldsymbol{n_1}.(\boldsymbol{C^2 n_1}) \tag{39}$$

If there were two preferred directions $\boldsymbol{n_1, n_2}$, this will introduce another set of invariants I_6, I_7

$$I_6 = \boldsymbol{n_2}.(\boldsymbol{C n_2}) \qquad I_7 = \boldsymbol{n_2}.(\boldsymbol{C^2 n_2}) \tag{40}$$

This also gives rise to a *coupling invariant* I_8

$$I_8 = \boldsymbol{n_1}.(\boldsymbol{C n_2}) = \boldsymbol{n_2}.(\boldsymbol{C n_1}) \tag{41}$$

Keeping all these in mind and focusing on the *orthotropy* and the laminar structure of the heart tissue as shown in Figure (9), we can write [9]

$$I_{4f} = \boldsymbol{f_0}.(\boldsymbol{C f_0}) \qquad I_{4s} = \boldsymbol{s_0}.(\boldsymbol{C s_0}) \qquad I_{4n} = \boldsymbol{n_0}.(\boldsymbol{C n_0}) \tag{42}$$

where

$$\sum_{i=f,s,n} I_{4i} = \boldsymbol{C}:(\boldsymbol{f_0} \otimes \boldsymbol{f_0} + \boldsymbol{s_0} \otimes \boldsymbol{s_0} + \boldsymbol{n_0} \otimes \boldsymbol{n_0}) = \boldsymbol{C}:\boldsymbol{I} = I_1 \tag{43}$$

That means only three of $I_1, I_{4f}, I_{4s}, I_{4n}$ are independent. Similarly I_{5f}, I_{5s}, I_{5n} are related as $I_{5f} + I_{5s} + I_{5n} = I_1^2 - 2I_2$. The coupling invariant I_8 is written as

$$I_{8\text{fs}} = I_{8\text{sf}} = \boldsymbol{f_0}.(\boldsymbol{C s_0}) \qquad I_{8\text{fn}} = I_{8\text{nf}} = \boldsymbol{f_0}.(\boldsymbol{C n_0}) \qquad I_{8\text{sn}} = I_{8\text{ns}} = \boldsymbol{n_0}.(\boldsymbol{C s_0}) \tag{44}$$

Furthermore,

$$I_{5f} = I_{4f}^2 + I_{8\text{fs}}^2 + I_{8\text{fn}}^2 \qquad I_{5s} = I_{4s}^2 + I_{8\text{fs}}^2 + I_{8\text{sn}}^2 \qquad I_{5n} = I_{4n}^2 + I_{8\text{fn}}^2 + I_{8\text{sn}}^2 \tag{45}$$

and

$$I_{4f}I_{4s}I_{4n} - I_{4f}I_{8\text{sn}}^2 - I_{4s}I_{8\text{fn}}^2 - I_{4n}I_{8\text{fs}}^2 + 2I_{8\text{fs}}I_{8\text{fn}}I_{8\text{sn}} = I_3 \tag{46}$$

Compiling this with the results from [4] (see Figure (9)) which showed that response is stiffest when the shear is in $\boldsymbol{f}$ direction, least stiff in $\boldsymbol{n}$ direction and intermediate in the $\boldsymbol{s}$ direction. There are differences in $\boldsymbol{fn}$ & $\boldsymbol{fs}$ and $\boldsymbol{sf}$ & $\boldsymbol{sn}$ responses, and not much difference between $\boldsymbol{nf}$ and $\boldsymbol{ns}$. To incorporate these into the material, we write the strain energy function as

$$W_{\text{iso}} = \frac{a}{2b}e^{[b(I_1-3)]} + \sum_{i=f,s} \frac{a_i}{2b_i}\{e^{[b_i(I_{4i}-1)^2]-1}\} + \frac{a_{\text{fs}}}{2b_{\text{fs}}}[e^{(b_{\text{fs}}I_{8\text{fs}}^2)-1}] \tag{47}$$

where on the right hand side, the first term is the *isotropic* term, second is the *transversely isotropic* term and the third is the *orthotropic* term. Now when we combine Eq. (37) and Eq. (47) as in Eq. (35),

$$W = \frac{a}{2b} e^{[b(I_1 - 3)]} + \sum_{i=f,s} \frac{a_i}{2b_i} \{ e^{[b_i(I_{4i}-1)^2]-1} \} + \frac{a_{\text{fs}}}{2b_{\text{fs}}} [e^{(b_{\text{fs}} I_{8\text{fs}}^2)-1}] + \kappa \left(\frac{(J-1)^2}{2} - \log J \right) \tag{48}$$

This describes the passive behavior of the heart muscle.

To describe the active behavior of the heart muscle, we take the stretch to be dependent only on one direction. This behavior can be described with strain energy function

$$W_{\text{act}} = T_a \left[\frac{\lambda^2}{2} - \lambda_0 \lambda \right] \tag{49}$$

where $\lambda = \sqrt{C_{11}}$ or $\sqrt{C_{22}}$ or $\sqrt{C_{33}}$ for each of the three mutually perpendicular directions.

Finally, combining both passive and active behavior,

$$W = \frac{a}{2b} e^{[b(I_1 - 3)]} + \sum_{i=f,s} \frac{a_i}{2b_i} \{ e^{[b_i(I_{4i}-1)^2]-1} \} + \frac{a_{\text{fs}}}{2b_{\text{fs}}} [e^{(b_{\text{fs}} I_{8\text{fs}}^2)-1}] + \kappa \left(\frac{(J-1)^2}{2} - \log J \right) + T_a \left[\frac{\lambda^2}{2} - \lambda_0 \lambda \right] \tag{50}$$

3.3 Test case - Nearly Incompressible Transversely Isotropic Hyperelastic material

Simulation of a *nearly incompressible*, *transversely isotropic* hyperelastic material is performed. An active part is also included. A 10mm x 10mm x 0.5mm domain is simulated. COMSOL's Solid Mechanics Physics is implemented in which Hyperelastic Material Model is chosen. Under the Hyperelastic Material Settings, user defined model is selected for Nearly Incompressible material with W_{iso} being the Isochoric Strain Energy Density and W_{vol} being the Volumetric Strain Energy Density. Active behaviour is also incorporated into W_{iso} as shown in the equations below. Two cases are simulated where the boundary conditions are given as (i) Fixed Constraint on one of the x-y plane faces and (ii) Fixed Constraint on one of the x-z plane faces, respectively. All the other faces are kept free to deform. Physics-controlled mesh of Normal size in COMSOL is used for meshing the domain (see Figure 20(a)). A Stationary Study is performed for each of the cases where the active force T_a is ramped up slowly using a ramp parameter for better convergence.

$$W = W_{\text{passive}} + W_{\text{act}} \tag{51}$$

$$W = W_{\text{iso}} + W_{\text{vol}} + W_{\text{act}} \tag{52}$$

$$W = \frac{a}{2b} e^{[b(I_1 - 3)]} + \kappa \left(\frac{(J-1)^2}{2} - \log J \right) + T_a \left[\frac{\lambda^2}{2} - \lambda_0 \lambda \right] \tag{53}$$

a	Material parameter	1.1481 kPa
b	Material parameter	3.8
κ	Material Parameter	1 GPa
λ	Fiber orientation parameter	$\sqrt{C_{11}}$
λ_0	Material parameter	0.5
T_a	Active Force	10 kPa

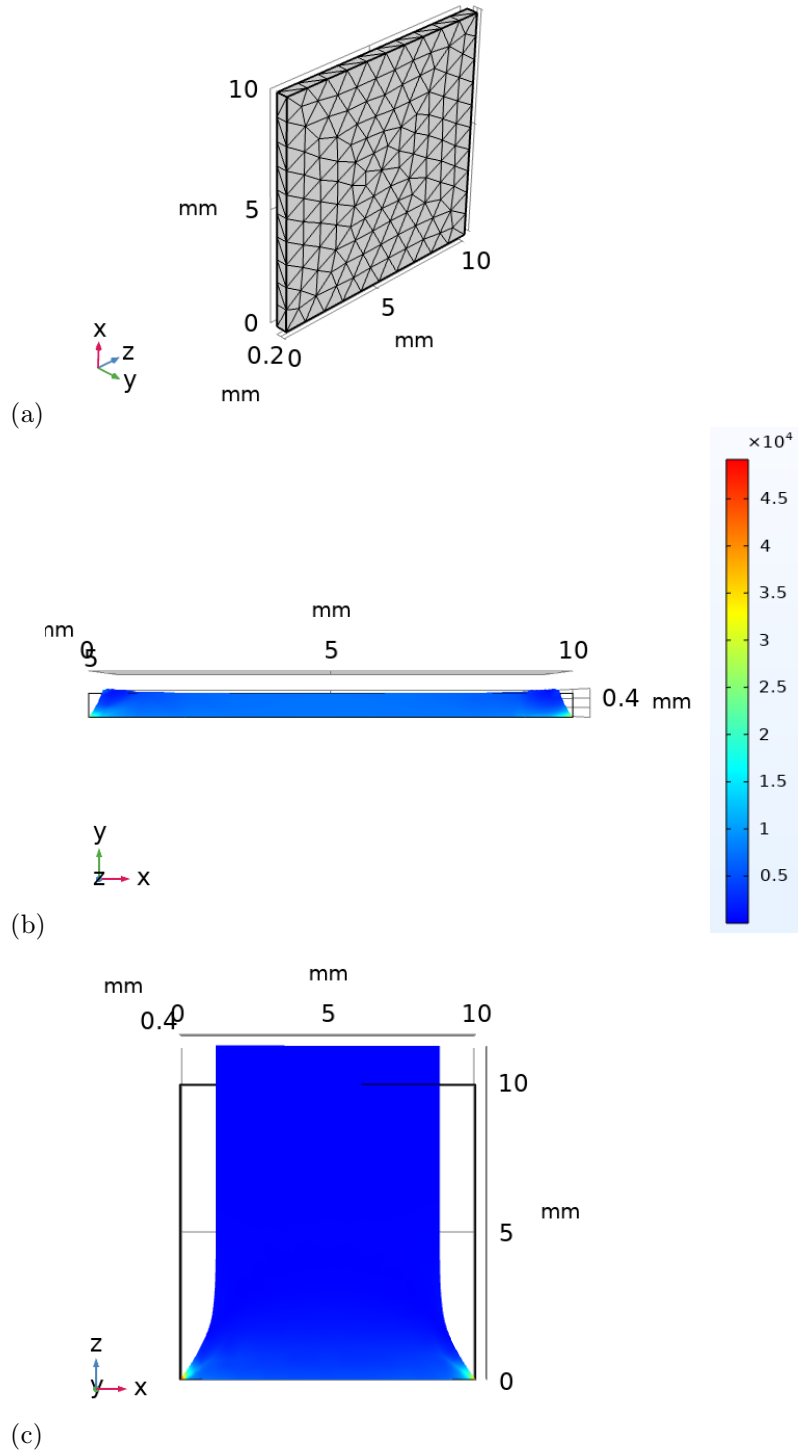**Table 1.** Constitutive equation parameters

(a)

(b)

(c)

Figure 20. Von-mises stress results of simulation of nearly incompressible transversely isotropic hyperelastic material. (a) Meshed domain. **(b)** Side view of the deformation when one of the faces along the z-x plane is fixed. **(c)** Top-view of the deformation when one of the faces along the y-x plane is fixed. The colour bar indicates Von-Mises stress in units of Pa.

Figure 20(b) and (c) show the deformation for each of the cases. Since the fiber orientation is in the x-direction, the deformation is significant along that direction. This is the evidence of the fact that fiber orientation plays a huge role in how the material behaves. In Figure 20(b), since the face in z-x plane is fixed and fiber orientation is along x-direction, deformation is negligible in the z-direction. Since the body is nearly incompressible, the body contracts along the x-direction and slightly stretched along y-drection. In Figure 20(c), the face in the y-x plane is fixed and fiber orientation being in x-direction, there is negligible deformation along y-direction. Again since the body is nearly incompressible, the only possible way for the body to deform is to contract along x-direction and elongate along z-direction.

In the above cases, the value of T_a is already defined in the model. But this active force arises from the contractile elements inside each of the myocytes. These contractile elements are activated by the action potential and hence the organic way of getting the value of T_a is to couple the action potential generation phenomena with the active force. This coupling will be covered in the next section.

4   Coupling of Electrophysiology and Solid Mechanics

In the previous sections, the electrophysiology and solid mechanics were dealt with independently. In this section, the dependency of one over the other will be introduced. In other words, both concepts will be coupled. In cardiac mechanics, there are two types of coupling: one-way and two-way coupling. In one-way coupling, only one of either electrophysiology or solid mechanics will depend on the other. In two-way coupling, both have effects on each other resulting in a feedback loop. In this thesis, only the one-way coupling will be covered where the propagation of action potential induces deformation in the domain. We have seen that the active contraction of the muscle cell happens because of the action potential propagation. So all that is required is to mathematically formulate the dependency of Active Force (T_a) on the Transmembrane Potential (V_m). This coupling can be looked at as a three part process,

   i. Solving Monodomain equations (12,13) to get the transmembrane potential (V_m) values

   ii. Using V_m from the above step to solve the transmembrane potential dependent active force (T_a) equation

   iii. Solving the solid mechanics equation with T_a from the above step

In contrast to Section 3.3 where T_a was given a user-defined value, here the value of T_a is obtained from solving the one-way coupling equation.

4.1   One-way coupling equation

As seen in Section 1.3.2, when the action potential propagates through a cardiac muscle cell, there is a mechanism which initiates the contraction of the cell. This contraction is not instantaneous. There is a delay between the action potential propagation and the induced contraction. This process can be portrayed with a mathematical expression used in [7],

$$\frac{\partial T_a}{\partial t} = \psi(V)[k(V - V_r) - T_a] \tag{54}$$

$$\psi(V) = \psi_0 + (\psi_\infty - \psi_0)e^{-e^{-\zeta(V - V_{\text{zero}})}} \tag{55}$$

Eq. (54) models the twitch-like response of the active force (T_a). $\frac{\partial T_a}{\partial t}$ vanishes when $T_a = k(V - V_r)$ where V_r is the resting potential. $\psi(V)$ is the rate-switch function defined as Eq. (55). Switch-rate function introduces the delay in the development of T_a with respect to V_m.

4.2   2D Test case – Nearly Incompressible Transversely Isotropic Hyperelastic material

A two-dimensional domain is subjected to stimulation to observe the propagation of the action potential leading to the induced contraction. A square domain of size 10mm x 10mm is simulated. Two different stimulation zones are tested: rectangular and circular.

$$\nabla.(-\sigma\nabla V_m) = -\beta\left(C_m\frac{\partial V_m}{\partial t} + i_{\text{ionic}}\right) + i_{\text{stim}}$$

$$\frac{\partial u}{\partial t} = e(V_m - du - b)$$

where,

$$i_{\text{ionic}} = c_1(V_m - a)(V_m - A)(V_m - B) + c_2 u(V_m - B)$$

The above set of monodomain equations are set up to simulate the action potential generation and propagation across the domain when stimulated. The simulation is performed for 0.6s with a time-step of 0.001s. A stimulus(i_{stim}) of magnitude $1000\,Am^{-3}$ is applied at $t = 0.01s$ (10 ms) for a duration of $0.001s$ (1 ms).
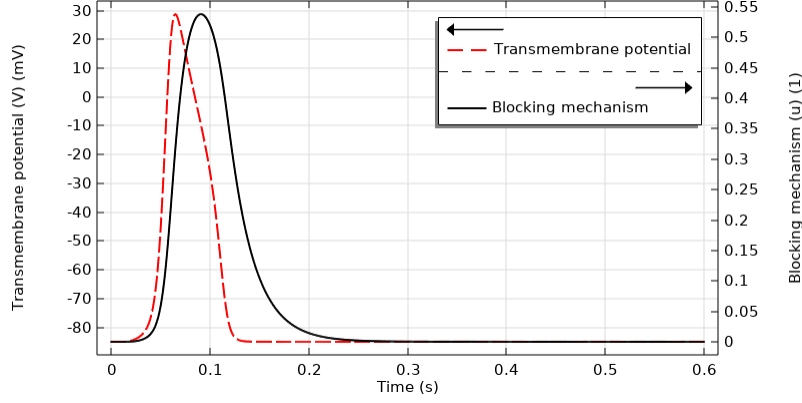

Figure 21. Plot of V_m and u Vs t. Left y-axis: Transmembrane potential (V_m). Right y-axis: Blocking Mechanism (u)

The solutions from the monodomain equations are used to solve the transmembrane potential dependent active force equation (one-way coupling equations):

$$\frac{\partial T_a}{\partial t} = \psi(V_m)[k(V_m - V_r) - T_a]$$

$$\psi(V_m) = \psi_0 + (\psi_\infty - \psi_0)e^{-e^{-\zeta(V_m - V_{\text{zero}})}}$$

It can be seen in the Figure 22 that there is a delay between the action potential and the active force.

V_r	Resting potential	-85 mV
V_{zero}	phase shift	0 mV
ψ_0	Rate constant of contraction	0.1 mV^{-1}
ψ_∞	Rate constant of contraction	1 mV^{-1}
k	Saturated active stress	0.005 MPa mV^{-1}
ζ	Transition rate	1 mV^{-1}

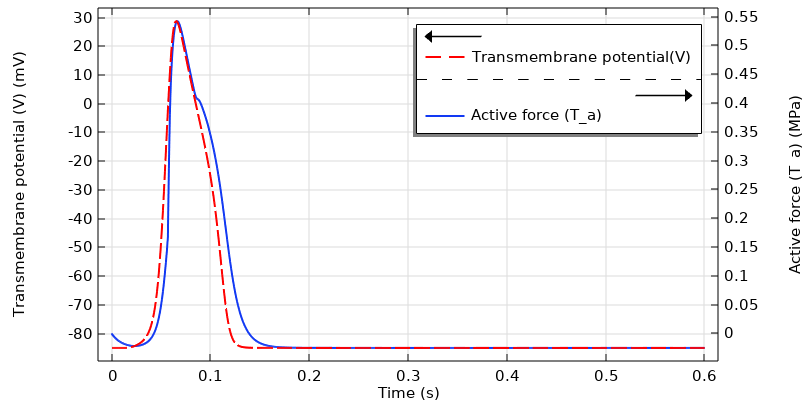**Table 2.** One-way coupling equation parameters

Figure 22. Plot of V_m and T_a Vs t.

We now know how the action potential propagates through the square domain and how it induces the active contraction in the domain. Final part is to incorporate these into the mechanical property of the heart muscle itself. This is done with the constitutive law for a Nearly Incompressible, Transversely Isotropic Hyperelastic material.

$$W = \frac{a}{2b}e^{[b(I_1-3)]} + \kappa\left(\frac{(J-1)^2}{2} - \log J\right) + T_a\left[\frac{\lambda^2}{2} - \lambda_0\lambda\right]$$

where λ is the direction of the fiber orientation. If $\lambda = \sqrt{C_{11}} \longrightarrow$ fiber orientaion in x-direction, $\lambda = \sqrt{C_{22}} \longrightarrow$ fiber orientation in y-direction and if $\lambda = \sqrt{C_{33}} \longrightarrow$ fiber orientation in z-direction.

COMSOL's General Form PDE is used to set-up the Monodomain equations. A Time Dependent Study is performed for $t = 0s$ to $t = 0.6s$ with step of $t = 0.001s$, to solve the Monodomain equations. The one-way coupling equation is also formulated using the General Form PDE. Another Time Dependent Study is performed for the same time instants as mentioned earlier, to solve the one-way coupling equation. While solving the one-way coupling equation, the values of V_m is taken from the solution of the Monodomain equations. In this way, we get the value of T_a and V_m at all space and time. Then, the Solid Mechanics Physics is set-up where the Hyperelastic material model is selected. These are solved by performing Stationary Study for each of the required time instant where the value of T_a is obtained from the previous study. Automatic highly nonlinear Newton method with maximum number of iteration=100 and tolerance factor =0.01 is used to solve the Solid Mechanics equations. Three cases are simulated: (i) Plane stimulus with fiber orientation in the x-direction, (ii) Plane stimulus with fiber orientation in the y-direction, and (iii) Radial stimulus with fiber orientation in the x-direction. Spring-type of boundary condition is applied to: (a) all the four outer edges of the domain with the isotropic spring constant per unit area $k_A = 10\text{Nm}^{-2}$, and (b) all the four corner points/vertices of the domain with the isotropic spring constant $k_A = 10\text{Nm}^{-1}$. Physics-controlled mesh of Normal size is used for meshing the domain in COMSOL.
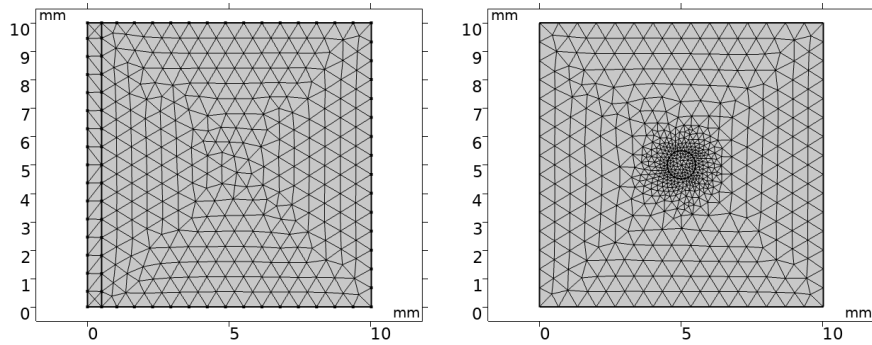

Figure 23. 2D meshed domain for (left) plane and (right) radial stimulus.

The results of the three simulation cases are shown in Figures 24,25,26. When the stimulus is applied to the region, that part gets depolarised. The value of V_m becomes less negative and keeps increasing. This results in the rise in the active force T_a too. The instant of depolarisation resulting in deformation can be seen in the $t = 0.012s$ snapshot in all the three figures. In Figure 24, since the fiber orientation is in x-direction, the regions with high V_m tend to contract the domain the x-direction which results in bulging at the end. At the peak of the action potential propagation which
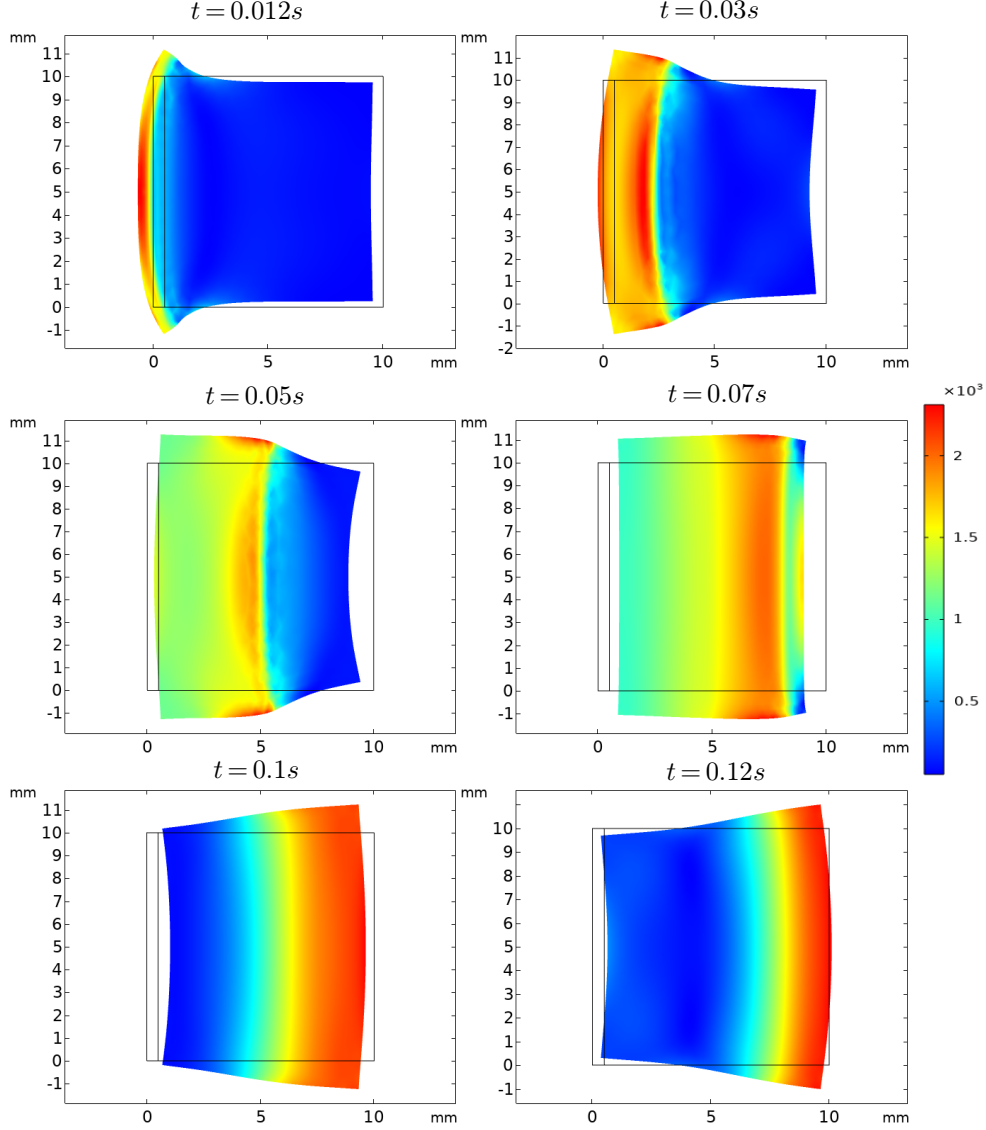
Figure 24. Plane stimulus with fiber orientation in the x-direction. Colour bar indicates Von-Mises stress.

is around $t = 0.07s$, the domain can be seen to be contracted to its maximum in the direction of the fiber orientation. In Figure 25, the fiber orientation is in the y-direction, so the propagating action potential leads to contraction of the domain in the y-direction. At $t = 0.07s$, the domain is contracted to its maximum in the y-direction. Similarly in Figure 26, the radial stimulus contracts the domain along the x-direction from both the sides and shows the maximum contraction at $t = 0.07s$ as expected. A similar analysis has been performed in [12], however in that paper the active stress is not anisotropic and the stimulus is a point source. This can be seen in Figure 27 where the action potential propagation is perfectly circular indicating the isotropic property. In this thesis, the active force is considered to be anisotropic which is the case in the actual heart muscle. As the action potential reaches its resting state, the trailing regions get repolarised and start to return to the original shape. This can be seen at $t = 0.12s$
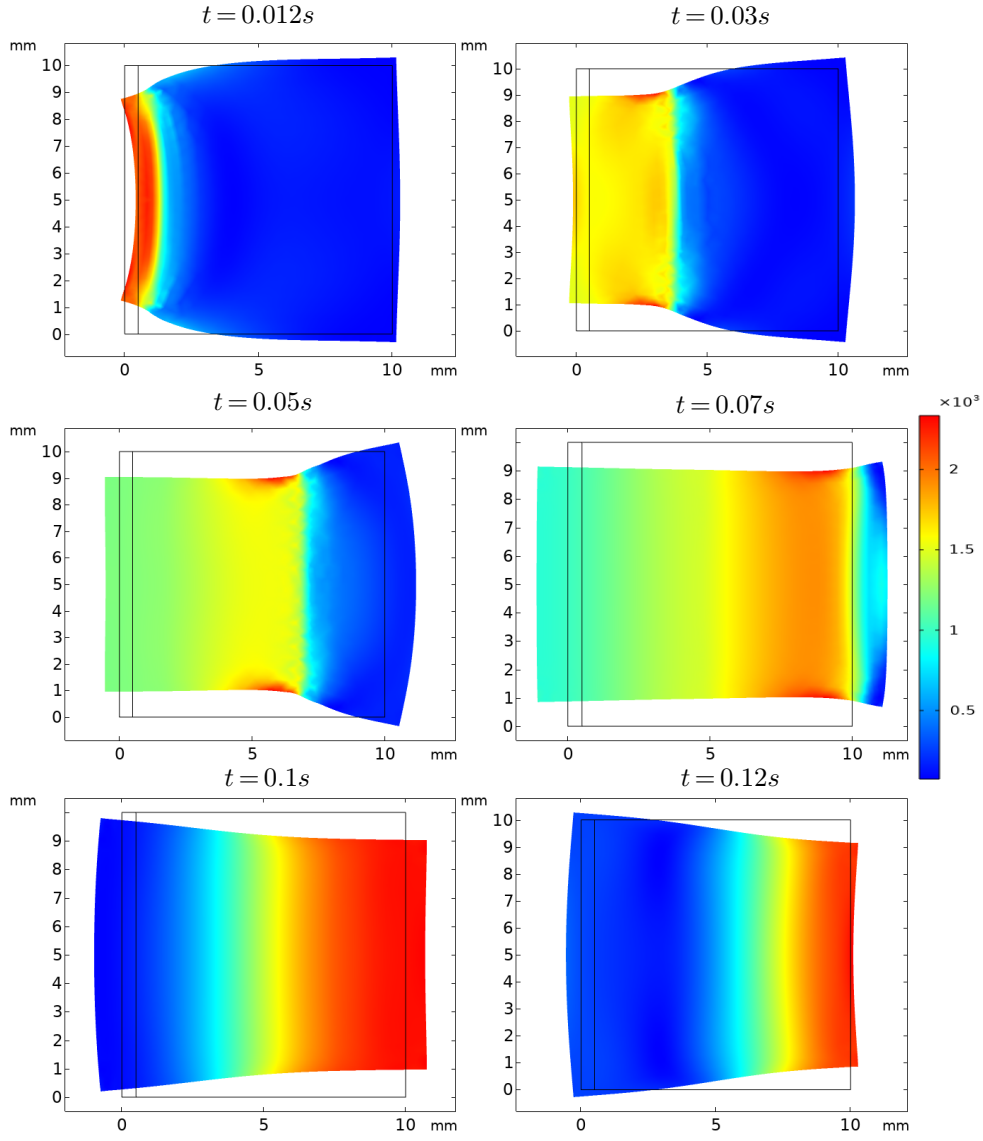
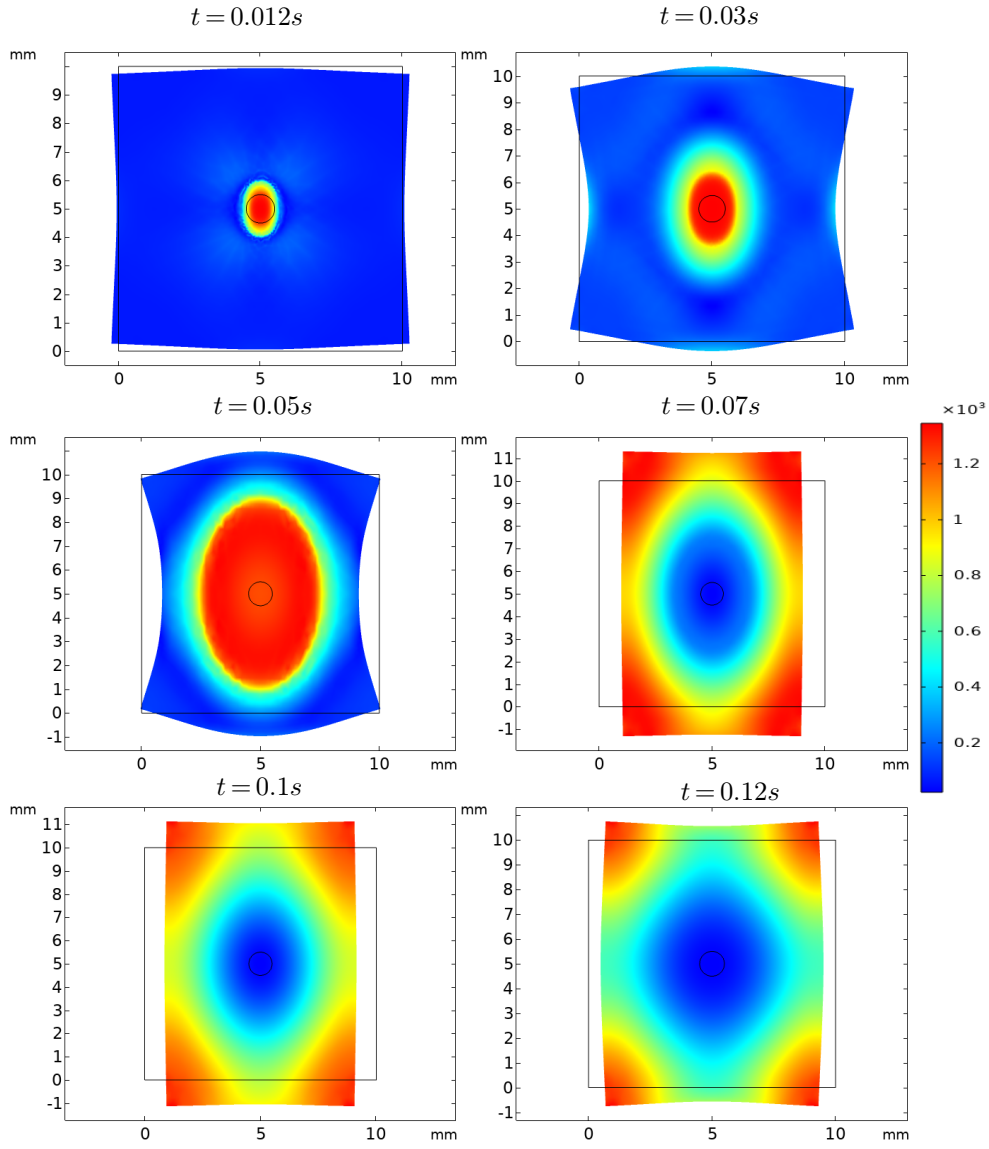**Figure 25.** Plane stimulus with fiber orientation in y-direction. Colour bar indicates Von-Mises stress.

Figure 26. Radial stimulus with fiber orientation in x-direction. Colour bar indicates Von-Mises stress.
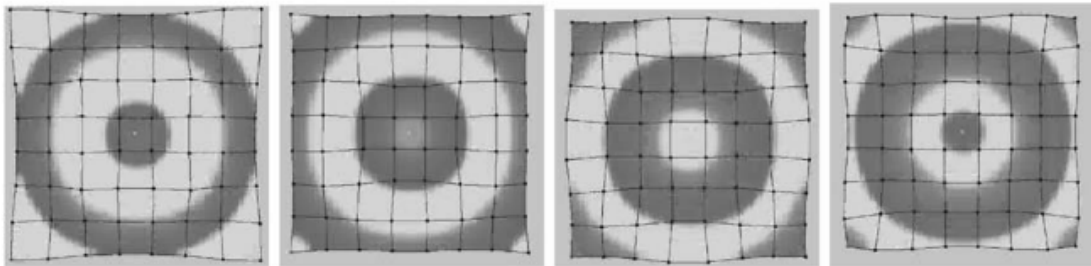

Figure 27. Deformation of an excitbale domain subjected to a point stimulus with a period of 310ms. The interval between the frames is 90ms. Taken from [12].

To get a better idea on how a single point is displaced due to the induced deformation, a point at (x,y)=(5mm,3mm) was taken and observed. Figure 28(c) shows the magnitude of the displacement of the point in the three different configurations, as time progresses. The radial stimulation shows the displacement to increase as the potential increases and then decrease as the potential decreases. For both plane stimulation, there are crests and troughs of rise and fall in the displacement magnitude. The plot shows us how, when the action potential propagates through the domain, a point gets displaced from its original position and return back. Figure 28(c) is a zoomed-in version of Figure 22, which can be used to compare the amount of displacement at various values of V_m and T_a.
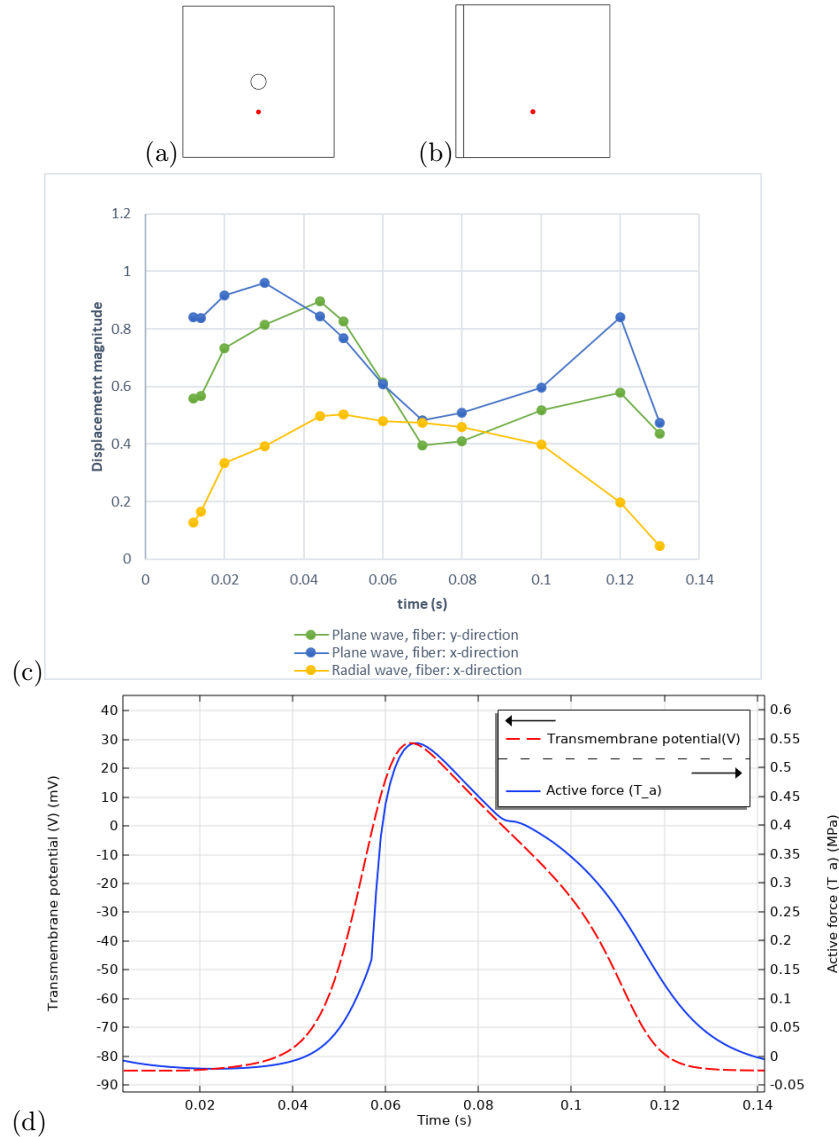

Figure 28. Displacement magnitude(in mm) of a point in the domain Vs time. **(a)** The point of interest at the position $(x, y) = (5\text{mm}, 3\text{mm})$ shown as a red dot in the domain with radial stimulus. **(b)** The point of interest at the position $(5\text{mm}, 3\text{mm})$ shown as a red dot in the domain with plane stimulus. **(c)** Plot of the magnitude of the displacement of the point(red dot) with time for different type of stimulus and fiber orientation. Displacement magnitude $=0$ means that the point remains at $(5\text{mm}, 3\text{mm})$. **(d)** V_m and T_a variation for the same time range, for comparison.

4.3 3D Test case – Nearly Incompressible Transversely Isotropic Hyper-elastic material

The analysis is extended from two dimensions to three dimensions. Here, a domain of size 10mm x 10mm x 0.5mm is simulated. The Monodomain and one-way coupling equations are again set-up with General form PDE and solved by performing Time Dependent studies. Similar to 2D, the one-way coupling equation is solved by taking V_m from the already solved Monodomain equations. Physics-controlled mesh with Extra Fine element size is used for meshing the domain (see Figure 29). Three cases are simulated here too: (i) Radial stimulus with fiber orientation along x-direction, (ii) Radial stimulus with fiber orientation along y-direction, and (iii) Plane stimulus with fiber orientation along x-direction. Spring-type boundary condition with isotropic sprint constant per unit volume $k_A = 1000 \mathrm{Nm}^{-3}$ is applied on all four 10mm x 0.5mm faces. Then the Solid Mechanics equation is solved by performing Stationary study similar to 2D. The active force T_a needs to be ramped slowly so that the simulations converge. So a ramping parameter is introduced. COMSOL's Automatic highly nonlinear Newton method is used to solve the equations.
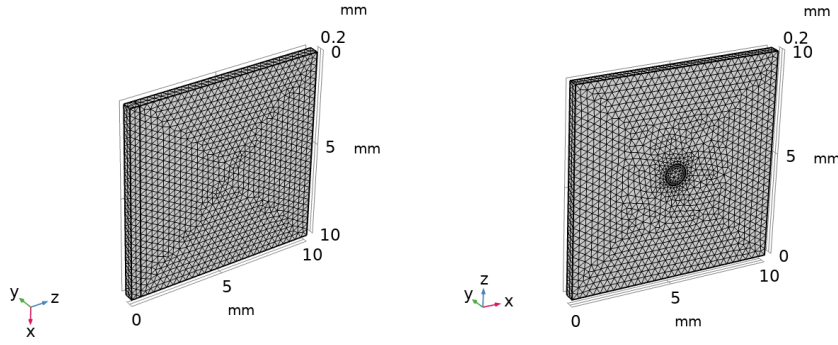

Figure 29. 3D meshed domain for (left) plane stimulus and (right) radial stimulus.

The results of each of the cases are shown in Figures 30,31,32. These results give us more and closer to real results when compared to the 2D results. First of all, 2D results do not tell us the stress distributions completely. It is not possible to gauge the exact dynamics from a 2D simulation. On the other hand, the 3D domains are closer to real-life models and the we can find out the stresses at each and every point in the domain to a certain accuracy. In Figure 30, we can see how the stresses start to build up right from the instant when the domain is stimulated. Since the fiber orientation is along the x-direction, we can instantly see the major deformation happening in that direction and the stresses being higher in those regions. Since the stimulus results in a radial action potential wave, the stress distribution also follows that shape. As time reaches $t = 0.07s$, around which V_m and T_a reach their peak, the radial distribution reaches all the faces of the domain resulting in a completely contracted geometry. As time further evolves, the domain starts to return back to its original dimensions.

In Figure 31, we see some interesting deformations. Here, the fiber orientation is in the y-direction which is normal to the plane of the body. As the domain is stimulated, there is initially a contraction of both faces on the x-z plane around the center ($t = 0.02s$). Then the whole domain gets blown out upwards along the y-axis (t=0.03s). As the action potential starts to spread towards

the boundaries, the domain returns to its original plane and gets stretched out in all four directions along the x-z plane ($t = 0.05s$). Later at $t = 0.09s$, there is some sort of an instability created due to which each of the pair of opposite corners move in different directions. Logically, as the action potential wave spreads out isotropically, the four corners should move in the same direction which is contrary to what is being observed. The cause of this needs to be investigated in detail.

Figure 32 shows the deformations for plane stimulus with fiber orientation along x-direction. The deformation follows the plane wave propagation and the contraction reaches the maximum at $t = 0.07s$ as expected. The domain also starts to return to its original dimensions at the end of the action potential propagation.
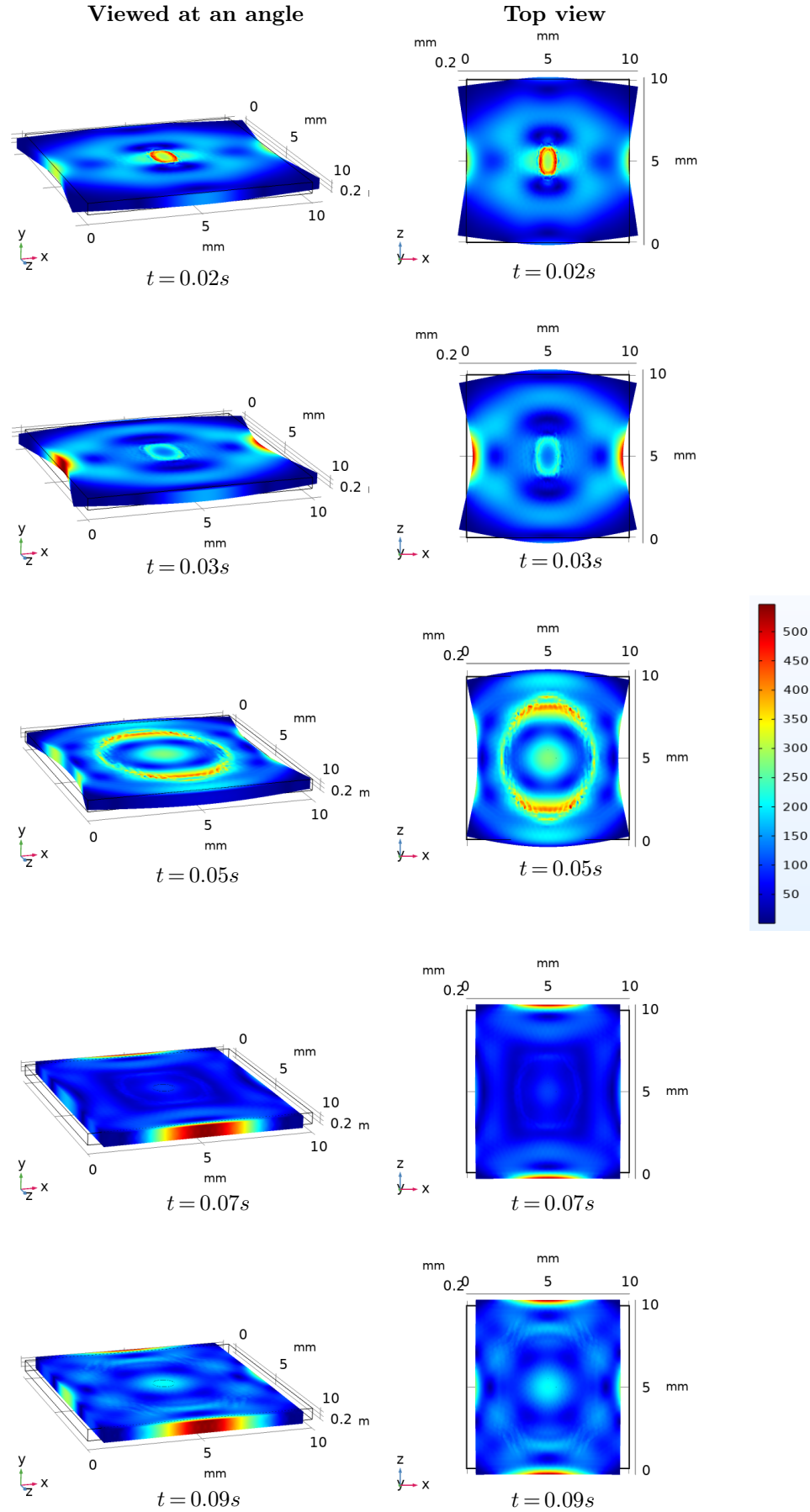
(intentionally left blank)

Viewed at an angle   **Top view**

Figure 30. Radial stimulus with fiber orientation in x-direction. Colour bar indicates Von-Mises stress.

Viewed from an angle   **Top View**
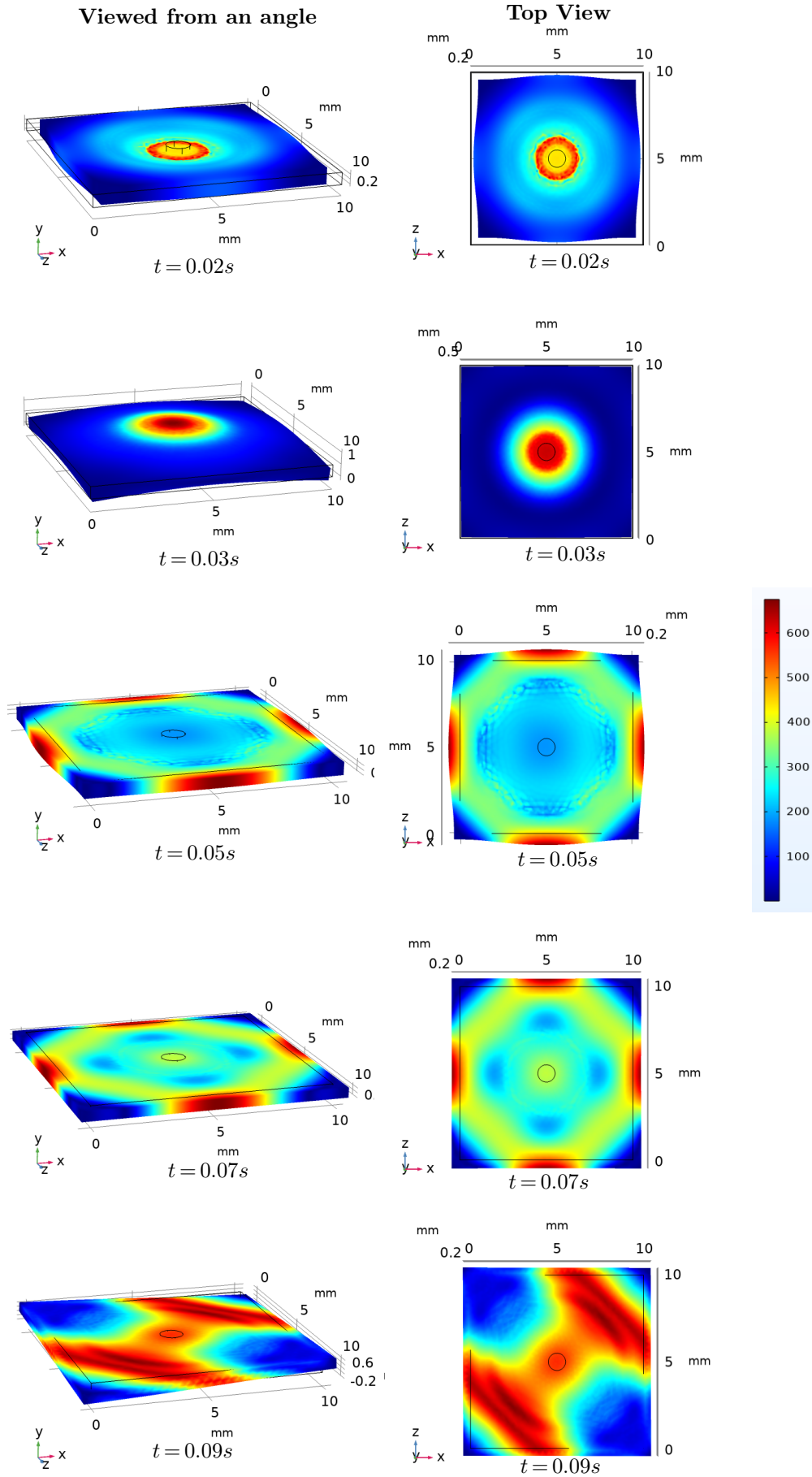
Figure 31. Radial stimulus with fiber orientation in y-direction. Colour bar indicates Von-Mises stress.

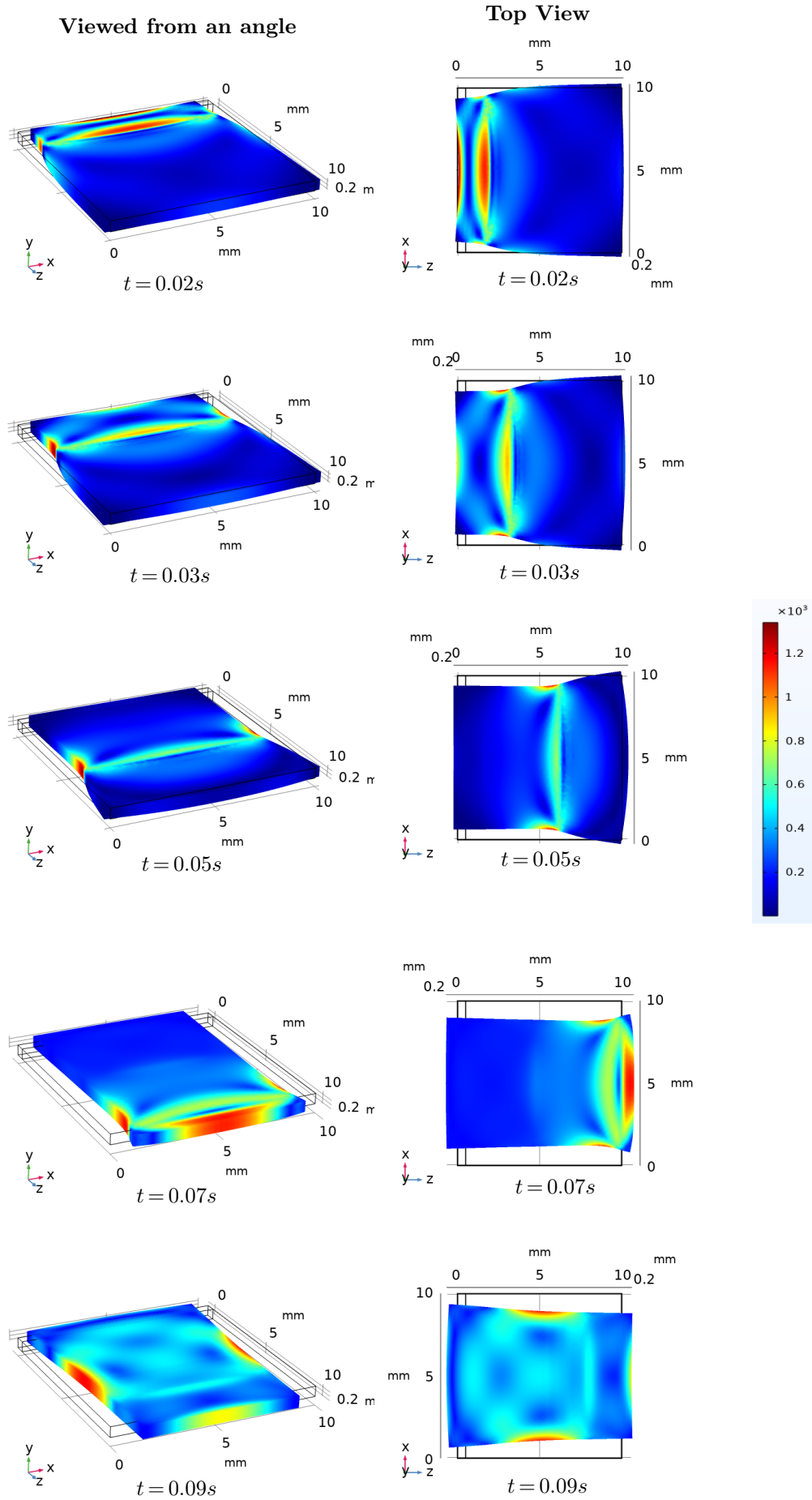**Viewed from an angle**   **Top View**

Figure 32. Plane stimulus with fiber orientation in x-direction. Colour bar indicates Von-Mises stress.

5 Conclusion and Further possibilities

The aim of this work has been to cover the need to model a heart, the concepts required to model it, and explore those models via simulations to gauge its usefulness. It covers the microscopic structure of the heart which includes the major contractile elements in the cardiomyocytes. The mechanism by which these contractile elements operate is explored via the generation and propagation of the action potential. This thesis discusses both Bidomain and Monodomain FHN models of the electrophysiology and dives into the monodomain simulation of the propagation of the action potential wave in two- and three- dimensions. The second part of the heart modelling includes the solid mechanics. All the necessary concepts leading to the properties of the heart muscle measured through various experimental tests are covered along with the theoretical framework of the passive and active deformation. Specifically, the Nearly Incompressible, Transversely Isotropic, Hyperelastic material model is considered for the simulations. Further, one-way coupling is introduced where the excitation induces deformation and the concepts of electrophysiology and solid mechanics are brought together here. Two- and three dimensional simulations of different stimulus types with varying fiber orientation is covered. The simulations show that the fiber orientation play a very important role and affects the way a body deforms significantly. The contraction is maximum in the direction of the fibers. Varying the conductivities also change the propagation velocity of the wave which, in turn affects the deformation.

The results in this thesis fairly match to the existing results from [7]. In that paper, the model is similar to that explored in this thesis, except the fact that the paper includes deformation induced excitation too. As seen in Figure 33, the deformations, after the initial load given to excite the domain, come close to the deformation in Figure 30. The initial deformation given to the domain in Figure 33 is equivalent to the external stimulus i_{stim} given to the domain in this thesis. Figure 34 shows only the excitation-induced deformation where the plane wave leads to a spiral wave reentry. Up until the point before reentry happens ($t = 420$ms), the deformations fairly match those in this thesis. This is a testament to the fact that the model seems to be giving good results and can be further improved.

This work only explores the coupling with transversely isotropic material property. The more accurate representation of the heart muscle is that it is orthotropic, the equations of which have been covered in this thesis (Eq. (50)). It contains three mutually perpendicular fibre orientations which affect the action potential propagation and in turn deformation. Simulations of the domain with orthotropic propoerty will be closer to a more accurate representation of the actual heart muscle. Also, simulation of spiral and scroll waves can also be explored for different material property and observe the differences in the results. Furthermore, the geometry of the domain can be extended to more life-like scenarios which could potentially have more impact in the real-world.
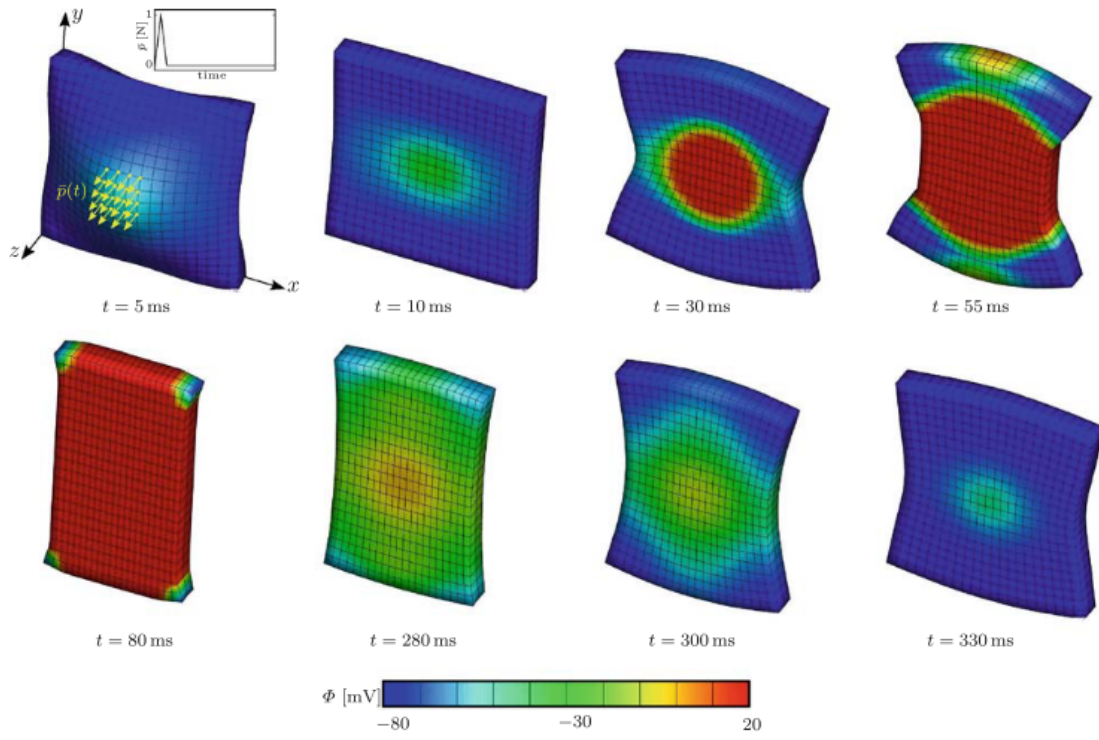
Figure 33. Deformation-induced excitation of deformable cardiac tissue. Snapshots of the deformed model depict the action potential contours at different stages of depolarization (upper row) and repolarization (lower row). Note that the cardiac tissue recovers its original shape at t = 0ms upon completion of repolarization at t ≈ 360 ms. Image and caption from [7].
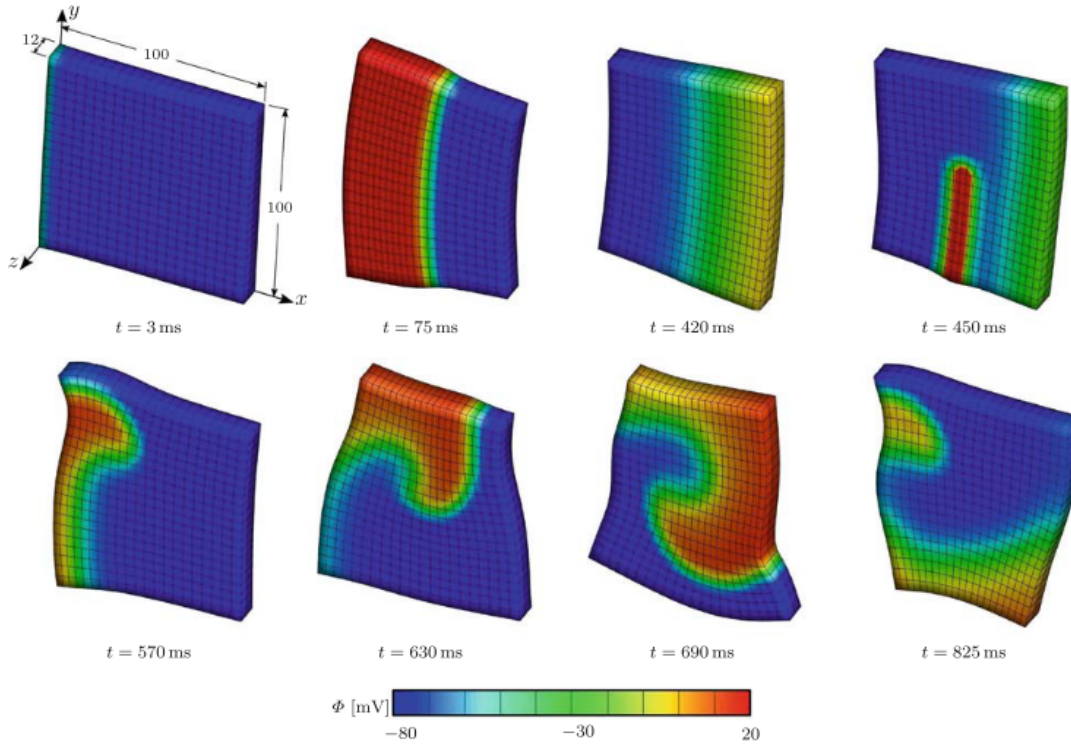

Figure 34. Initiation and rotation of scroll re-entry in excitable and deformable cardiac tissue. Image and caption from [7].

Bibliography

[1] Jazmin Aguado-Sierra, Adarsh Krishnamurthy, Christopher Villongco, Joyce Chuang, Elliot Howard, Matthew J Gonzales, Jeff Omens, David E Krummen, Sanjiv Narayan, Roy CP Kerckhoffs et al. Patient-specific modeling of dyssynchronous heart failure: a case study. *Progress in biophysics and molecular biology*, 107(1):147–155, 2011.

[2] RH Clayton and AV Panfilov. A guide to modelling cardiac electrical activity in anatomically detailed ventricles. *Progress in biophysics and molecular biology*, 96(1-3):19–43, 2008.

[3] Socrates Dokos. *Modelling organs, tissues, cells and devices: using MATLAB and COMSOL multiphysics*. Springer, 2017.

[4] Socrates Dokos, Bruce H Smaill, Alistair A Young, and Ian J LeGrice. Shear properties of passive ventricular myocardium. *American Journal of Physiology-Heart and Circulatory Physiology*, 283(6):0, 2002.

[5] Richard FitzHugh. Impulses and physiological states in theoretical models of nerve membrane. *Biophysical journal*, 1(6):445–466, 1961.

[6] YC Fung. Elasticity of soft tissues in simple elongation. *American Journal of Physiology-Legacy Content*, 213(6):1532–1544, 1967.

[7] Serdar Göktepe and Ellen Kuhl. Electromechanics of the heart: a unified approach to the strongly coupled excitation–contraction problem. *Computational Mechanics*, 45(2):227–243, 2010.

[8] Alan L Hodgkin and Andrew F Huxley. A quantitative description of membrane current and its application to conduction and excitation in nerve. *The Journal of physiology*, 117(4):500–544, 1952.

[9] Gerhard A Holzapfel and Ray W Ogden. Constitutive modelling of passive myocardium: a structurally based framework for material characterization. *Philosophical Transactions of the Royal Society A: Mathematical, Physical and Engineering Sciences*, 367(1902):3445–3475, 2009.

[10] Adarsh Krishnamurthy, Christopher T Villongco, Joyce Chuang, Lawrence R Frank, Vishal Nigam, Ernest Belezzuoli, Paul Stark, David E Krummen, Sanjiv Narayan, Jeffrey H Omens et al. Patient-specific models of cardiac biomechanics. *Journal of computational physics*, 244:4–21, 2013.

[11] Jinichi Nagumo, Suguru Arimoto, and Shuji Yoshizawa. An active pulse transmission line simulating nerve axon. *Proceedings of the IRE*, 50(10):2061–2070, 1962.

[12] Martyn P Nash and Alexander V Panfilov. Electromechanical model of excitable tissue to study reentrant cardiac arrhythmias. *Progress in biophysics and molecular biology*, 85(2-3):501–522, 2004.

[13] World Health Organization et al. *Global status report on noncommunicable diseases 2014*. Number WHO/NMH/NVI/15.1. World Health Organization, 2014.

[14] John G Pinto and YC Fung. Mechanical properties of the heart muscle in the passive state. *Journal of biomechanics*, 6(6):597–616, 1973.

[15] Alfio Quarteroni, Toni Lassila, Simone Rossi, and Ricardo Ruiz-Baier. Integrated heart—coupling multiscale and multiphysics models for the simulation of the cardiac function. *Computer Methods in Applied Mechanics and Engineering*, 314:345–407, 2017.

[16] Jack M Rogers and Andrew D McCulloch. A collocation-galerkin finite element model of cardiac action potential propagation. *IEEE Transactions on Biomedical Engineering*, 41(8):743–757, 1994.

[17] Larry A Taber. *Continuum Modeling in Mechanobiology*. Springer, 2020.

[18] Hugo Talbot, Stéphanie Marchesseau, Christian Duriez, Maxime Sermesant, Stéphane Cotin, and Hervé Delingette. Towards an interactive electromechanical model of the heart. *Interface focus*, 3(2):20120091, 2013.

[19] Dominique Vervoort, Bart Meuris, Bart Meyns, and Peter Verbrugghe. Global cardiac surgery: access to cardiac surgical care around the world. *The Journal of thoracic and cardiovascular surgery*, 159(3):987–996, 2020.

[20] Andrew L Wit, Hein J Wellens, and Mark E Josephson. *Electrophysiological Foundations of Cardiac Arrhythmias: A Bridge Between Basic Mechanisms and Clinical Electrophysiology*. Cardiotext Publishing, 2017.

[21] Frank CP Yin, Robert K Strumpf, Paul H Chew, and Scott L Zeger. Quantification of the mechanical properties of noncontracting canine myocardium under simultaneous biaxial loading. *Journal of biomechanics*, 20(6):577–589, 1987.